MIXED DISCONTINUOUS GALERKIN APPROXIMATION OF THE MAXWELL OPERATOR

PAUL HOUSTON *, ILARIA PERUGIA †, AND DOMINIK SCHÖTZAU ‡

Abstract. We introduce and analyze a discontinuous Galerkin discretization of the Maxwell operator in mixed form. Here, all the unknowns of the underlying system of partial differential equations are approximated by discontinuous finite element spaces of the same order. For piecewise constant coefficients, the method is shown to be stable and optimally convergent with respect to the mesh size. Numerical experiments highlighting the performance of the proposed method for problems with both smooth and singular analytical solutions are presented.

Key words. Discontinuous Galerkin methods, mixed methods, Maxwell operator

AMS subject classifications. 65N30

1. Introduction. The origins of discontinuous Galerkin (DG) methods can be traced back to the seventies, where they were proposed for the numerical solution of the neutron transport equation, as well as for the weak enforcement of continuity in Galerkin methods for elliptic and parabolic problems; see [12] for a historical review. In the meantime, these methods have undergone quite a remarkable development and are used in a wide range of applications; see the recent survey articles [10, 13, 14] and the references cited therein. The main advantages of DG methods lie in their robustness, conservation properties and great flexibility in the mesh-design. Indeed, being based on completely discontinuous finite element spaces, these methods can easily handle elements of various types and shapes, non-matching grids and local spaces of different polynomial orders; thus, they are ideal for *hp*-adaptivity.

In recent years, DG methods have begun to find their way into computational electromagnetics. Here, we mention the work in [31], where the full Maxwell system is discretized using unstructured spectral elements in space together with a suitable low-storage Runge-Kutta time stepping scheme. Similar discontinuous spectral Galerkin methods were proposed in [21]. The study of DG methods applied to the time-harmonic Maxwell equations in electric field-based formulation was initiated in [24], where a local discontinuous Galerkin (LDG) method was proposed for the low-frequency approximation of these equations, covering the cases of heterogeneous media and topologically non-trivial domains. The numerical experiments in [19] have confirmed the optimal *hp*-convergence rates proved in [24] for smooth solutions, and indicate that DG methods can be effective in a wide range of low-frequency applications where the bilinear forms are coercive.

On the other hand, one of the main difficulties in the numerical solution of Maxwell's equations consists in dealing with divergence-free constraints that need to be imposed on the fields, especially in cases where the exact solutions exhibit strong singularities. Several approaches have been proposed in the literature: we mention here the (weighted) regularization method studied in [1, 15], the singular

* Department of Mathematics and Computer Science, University of Leicester, Leicester LE1 7RH, UK, email: `Paul.Houston@mcs.le.ac.uk`.

†Dipartimento di Matematica, Università di Pavia, Via Ferrata 1, 27100 Pavia, Italy, email: `perugia@dimat.unipv.it`.

‡Department of Mathematics, University of Basel, Rheinsprung 21, 4051 Basel, Switzerland, email: `schotzau@math.unibas.ch`. Partially supported by the Swiss National Science Foundation under Project 21-068126.02.

field approach of [5], and the Lagrange multiplier techniques used in [8, 16, 30] (see also the references cited therein). The methods studied in [24, 19] are DG versions of the regularization approach of [1] and, for singular solutions, were shown to suffer from similar drawbacks as their conforming counterparts. A mixed discontinuous Galerkin approach was recently adopted in [25], where a stabilized interior penalty discretization was proposed for the high-frequency time-harmonic Maxwell equations. For smooth material coefficients, optimal convergence of the method was proved by employing a duality approach, provided that appropriate stabilization terms were included in the method.

In this paper, we introduce and analyze a new mixed DG formulation for the Maxwell operator (consisting of the curl-curl operator subject to a divergence-free constraint). Although this formulation is based on the same mixed approach as the one proposed in [25], here the amount of numerical stabilization is drastically reduced. In particular, we abandon all the volume stabilization terms from [25] and achieve well-posedness of the formulation through a suitable definition of the numerical fluxes. We present a numerical analysis of this method for piecewise constant material coefficients, and obtain a priori error bounds in the associated energy norm that are optimal in the mesh size, if both the field and the Lagrange multiplier related to the divergence constraint are approximated with piecewise polynomials of the same degree. Here, we consider both the case where the underlying analytical solution is smooth and where only minimal regularity assumptions are assumed. The method proposed in this paper is tested on a set of numerical examples that confirm the convergence rates predicted in the theoretical analysis, for both smooth and singular solutions on regular and irregular meshes. The method is also tested within an adaptive procedure on affine quadrilateral meshes where hanging nodes are introduced during the course of the refinement. The numerical results indicate that singularities present in the analytical solution are correctly captured by the proposed scheme.

The stability analysis of the mixed DG formulation is carried out along the following lines. First of all, we rewrite the mixed system in an augmented form by introducing auxiliary variables. This results in a standard mixed saddle point problem with nonconforming forms. Then, we establish coercivity of the curl-curl operator on a suitable kernel. To prove the inf-sup stability condition for the form related to the divergence constraint, we use a norm-equivalence property for DG spaces (similar techniques were employed in [22] to investigate conservation properties of DG methods) and, following ideas from [7], we invoke stability properties of the underlying (stable) conforming spaces. Finally, we note that, although the method here is very similar to the mixed discontinuous Galerkin methods proposed, e.g., in [11, 18, 29, 28] for the Stokes equations of incompressible fluid flow, our analysis differs considerably from the approaches there, mainly due to the fact that the curl-curl operator has a large kernel and that the multiplier is H^1–continuous.

The outline of the paper is as follows: in Section 2 we introduce our mixed DG method for the Maxwell operator. Our main theoretical results are the a priori error bounds presented in Section 3. Their proofs are carried out in the following sections by introducing an auxiliary mixed formulation (Section 4), by establishing continuity and stability properties of the forms that are involved (Section 5), and finally by deriving the actual error estimates (Section 6). The numerical performance of the method is tested in Section 7. Concluding remarks are presented in Section 8. In the appendix, we prove a crucial norm-equivalence property.

2. Mixed DG discretization of the Maxwell operator. In this section, we introduce a mixed DG discretization of the curl-curl operator subject to a divergence-free constraint.

2.1. Notation. We start by introducing the notation and function spaces that will be used throughout this paper. Given a bounded domain D in $\mathbb{R}^2$ or $\mathbb{R}^3$, we denote by $H^s(D)$ the standard Sobolev space of functions with integer or fractional regularity exponent $s \geq 0$, and by $\|\cdot\|_{s,D}$ its norm. We also write $\|\cdot\|_{s,D}$ to denote the norms in the spaces $H^s(D)^d$, $d = 2, 3$. We set $L^2(D) = H^0(D)$. Furthermore, $L^\infty(D)$ is the space of bounded functions on D, with norm $\|\cdot\|_{\infty,D}$. Given $D \subset \mathbb{R}^3$ and a positive weight function $w \in L^\infty(D)$, $H(\mathrm{curl}_w; D)$ and $H(\mathrm{div}_w; D)$ are the spaces of vector fields $\boldsymbol{u} \in L^2(D)^3$ with $\nabla \times (w\boldsymbol{u}) \in L^2(D)^3$ and $\nabla \cdot (w\boldsymbol{u}) \in L^2(D)$, respectively, endowed with their corresponding graph norms. For $w \equiv 1$, we omit the subscript and write $H(\mathrm{curl}; D)$ and $H(\mathrm{div}; D)$, respectively. We denote by $H_0^1(D)$, $H_0(\mathrm{curl}_w; D)$ and $H_0(\mathrm{div}_w; D)$ the subspaces of $H^1(D)$, $H(\mathrm{curl}_w; D)$ and $H(\mathrm{div}_w; D)$, respectively, of functions with zero trace, tangential trace and normal trace, respectively, and by $H(\mathrm{curl}_w^0; D)$ and $H(\mathrm{div}_w^0; D)$ the subspaces of $H(\mathrm{curl}_w; D)$ and $H(\mathrm{div}_w; D)$, respectively, of functions with zero (weighted) curl and divergence, respectively. Finally, we set $H_0(\mathrm{curl}_w^0; D) = H(\mathrm{curl}_w^0; D) \cap H_0(\mathrm{curl}_w, D)$ and $H_0(\mathrm{div}_w^0; D) = H(\mathrm{div}_w^0; D) \cap H_0(\mathrm{div}_w, D)$.

2.2. Model problem. We consider the following mixed model problem: find the vector field $\boldsymbol{u}$ and the scalar field p such that

$$\begin{aligned} \nabla \times (\mu^{-1} \nabla \times \boldsymbol{u}) - \varepsilon \nabla p &= \boldsymbol{j} \quad \text{in } \Omega, \\ \nabla \cdot (\varepsilon \boldsymbol{u}) &= 0 \quad \text{in } \Omega, \\ \boldsymbol{n} \times \boldsymbol{u} &= \boldsymbol{g} \quad \text{on } \Gamma, \\ p &= 0 \quad \text{on } \Gamma. \end{aligned} \tag{2.1}$$

Here, Ω is a bounded Lipschitz polyhedron in $\mathbb{R}^3$, with $\boldsymbol{n}$ denoting the outward normal unit vector to its boundary $\Gamma = \partial\Omega$. The right-hand side $\boldsymbol{j} \in L^2(\Omega)^3$ in the first equation is an external source field, and the Dirichlet datum $\boldsymbol{g}$ is a prescribed tangential trace which we assume to belong to $L^2(\Gamma)^3$. We further assume that the domain Ω is simply-connected, and that Γ is connected. The coefficients $\mu = \mu(\boldsymbol{x})$ and $\varepsilon = \varepsilon(\boldsymbol{x})$ are real functions in $L^\infty(\Omega)$ that satisfy

$$0 < \mu_* \leq \mu(\boldsymbol{x}) \leq \mu^* < \infty, \qquad 0 < \varepsilon_* \leq \varepsilon(\boldsymbol{x}) \leq \varepsilon^* < \infty, \quad \text{a.e. } \boldsymbol{x} \in \overline{\Omega}, \tag{2.2}$$

respectively. For simplicity, we assume that μ and ε are piecewise constant and that there is a partition of the domain Ω into Lipschitz polyhedra such that μ and ε are constant in each of them.

REMARK 2.1. *Problem (2.1) describes the principal operator of the time-harmonic Maxwell equations in a heterogeneous insulating medium (i.e., with electric conductivity $\sigma = 0$). The coefficients μ and ε are the magnetic permeability and the electric permittivity of the medium, respectively. The divergence constraint is incorporated by means of the Lagrange multiplier p; see, e.g., [16, 25, 30] and the references cited therein for details. Problem (2.1) is also a formulation of the magnetostatic problem in terms of the vector potential $\boldsymbol{u}$ and with Coulomb's gauge $\nabla \cdot \boldsymbol{u} = 0$ ($\varepsilon \equiv 1$ in this case).*

Set $\boldsymbol{V} = \{\boldsymbol{v} \in H(\mathrm{curl}; \Omega) : (\boldsymbol{n} \times \boldsymbol{v})|_\Gamma \in L^2(\Gamma)^3\}$ and $Q = H_0^1(\Omega)$. The standard variational form of problem (2.1) consists in finding $\boldsymbol{u} \in \boldsymbol{V}$, with $\boldsymbol{n} \times \boldsymbol{u} = \boldsymbol{g}$ on Γ, and $p \in Q$ such that

$$\begin{aligned} a(\boldsymbol{u},\boldsymbol{v}) + b(\boldsymbol{v},p) &= f(\boldsymbol{v}), && (2.3)\\ b(\boldsymbol{u},q) &= 0 && (2.4)\end{aligned}$$

for any $(\boldsymbol{v},q) \in H_0(\mathrm{curl};\Omega)\times Q$, where the forms a and b and the functional f are given by

$$\begin{aligned} a(\boldsymbol{u},\boldsymbol{v}) &= \int_\Omega \mu^{-1}\nabla\times\boldsymbol{u}\cdot\nabla\times\boldsymbol{v}\,d\boldsymbol{x},\\ b(\boldsymbol{v},p) &= -\int_\Omega \varepsilon\boldsymbol{v}\cdot\nabla p\,d\boldsymbol{x},\\ f(\boldsymbol{v}) &= \int_\Omega \boldsymbol{j}\cdot\boldsymbol{v}\,d\boldsymbol{x} - \int_\Gamma \boldsymbol{g}\cdot\mu^{-1}\nabla\times\boldsymbol{v}\,ds.\end{aligned}$$

Well-posedness of the formulation (2.3)–(2.4) follows from the standard theory of mixed problems [6], since a is bilinear, continuous and coercive on the kernel of b, and b is linear and continuous, and satisfies the inf-sup condition; see, e.g., [30] for details.

2.3. Meshes, finite element spaces and traces. We consider shape regular meshes $\mathcal{T}_h$ that partition the domain Ω into tetrahedra and/or parallelepipeds, with possible hanging nodes; we always assume that the meshes are aligned with any discontinuities in the coefficients μ and ε. Each element is affinely equivalent to a reference element $\widehat{K}$ which is either the tetrahedron $\{\hat{x}_1,\hat{x}_2,\hat{x}_3>0,\ \hat{x}_1+\hat{x}_2+\hat{x}_3<1\}$ or the cube $(0,1)^3$. We denote by h_K the diameter of the element $K\in\mathcal{T}_h$ and set $h=\max_K h_K$. An interior face of $\mathcal{T}_h$ is defined as the (non-empty) two-dimensional interior of $\partial K^+\cap\partial K^-$, where K^+ and K^- are two adjacent elements of $\mathcal{T}_h$, not necessarily matching. A boundary face of $\mathcal{T}_h$ is defined as the (non-empty) two-dimensional interior of $\partial K\cap\Gamma$, where K is a boundary element of $\mathcal{T}_h$. We denote by $\mathcal{F}_h^{\mathcal{I}}$ the union of all interior faces of $\mathcal{T}_h$, by $\mathcal{F}_h^{\mathcal{D}}$ the union of all boundary faces of $\mathcal{T}_h$, and set $\mathcal{F}_h=\mathcal{F}_h^{\mathcal{I}}\cup\mathcal{F}_h^{\mathcal{D}}$.

Given a nonnegative integer ℓ and an element $K\in\mathcal{T}_h$, we define $\mathcal{S}^\ell(K)$ as the space $\mathcal{P}^\ell(K)$ of polynomials of degree at most ℓ in K, if K is a tetrahedron, or the space $\mathcal{Q}^\ell(K)$ of polynomials of degree at most ℓ in each variable in K, if K is a parallelepiped. Similarly, for a face $f\in\mathcal{F}_h$, we write $\mathcal{S}^\ell(f)$ for the space $\mathcal{P}^\ell(f)$ of polynomials of degree at most ℓ in f, if f is a triangle, and the space $\mathcal{Q}^\ell(f)$ of polynomials of degree at most ℓ in each variable in f, if f is a parallelogram. Then, the generic finite element space of discontinuous piecewise polynomials is given by

$$S^\ell(\mathcal{T}_h) := \{u\in L^2(\Omega):\ u|_K\in\mathcal{S}^\ell(K)\ \ \forall K\in\mathcal{T}_h\}.$$

For piecewise smooth vector- and scalar-valued functions $\boldsymbol{v}$ and q, respectively, we introduce the following trace operators. Let $f\subset\mathcal{F}_h^{\mathcal{I}}$ be an interior face shared by two neighboring elements K^+ and K^-, we write $\boldsymbol{n}^\pm$ to denote the outward normal unit vectors to the boundaries $\partial K^\pm$, respectively. Denoting by $\boldsymbol{v}^\pm$ and $q^\pm$ the traces of $\boldsymbol{v}$ and q on $\partial K^\pm$ taken from within $K^\pm$, respectively, we define the jumps across f by

$$\begin{aligned} [\![\boldsymbol{v}]\!]_T &= \boldsymbol{n}^+\times\boldsymbol{v}^+ + \boldsymbol{n}^-\times\boldsymbol{v}^-, \qquad [\![\boldsymbol{v}]\!]_N = \boldsymbol{v}^+\cdot\boldsymbol{n}^+ + \boldsymbol{v}^-\cdot\boldsymbol{n}^-,\\ [\![q]\!]_N &= q^+\boldsymbol{n}^+ + q^-\boldsymbol{n}^-,\end{aligned}$$

and the averages by

$$\{\!\{\boldsymbol{v}\}\!\} = (\boldsymbol{v}^+ + \boldsymbol{v}^-)/2, \qquad \{\!\{q\}\!\} = (q^+ + q^-)/2.$$

On a boundary face $f\subset\mathcal{F}_h^{\mathcal{D}}$, we set $[\![\boldsymbol{v}]\!]_T=\boldsymbol{n}\times\boldsymbol{v}$, $[\![q]\!]_N=q\,\boldsymbol{n}$, $\{\!\{\boldsymbol{v}\}\!\}=\boldsymbol{v}$ and $\{\!\{q\}\!\}=q$.

2.4. DG discretization. We wish to approximate problem (2.1) by discrete functions $\boldsymbol{u}_h$ and p_h in the finite element spaces

$$\boldsymbol{V}_h = S^\ell(\mathcal{T}_h)^3 \quad \text{and} \quad Q_h = S^\ell(\mathcal{T}_h),$$

respectively, for a given partition $\mathcal{T}_h$ of Ω, and an approximation order $\ell \geq 1$.

To this end, we consider the following DG method: find $(\boldsymbol{u}_h, p_h) \in \boldsymbol{V}_h \times Q_h$ such that

$$a_h(\boldsymbol{u}_h, \boldsymbol{v}) + b_h(\boldsymbol{v}, p_h) = f_h(\boldsymbol{v}), \tag{2.5}$$

$$b_h(\boldsymbol{u}_h, q) \ - c_h(p_h, q) = 0, \tag{2.6}$$

for any $(\boldsymbol{v}, q) \in \boldsymbol{V}_h \times Q_h$, where the discrete forms a_h, b_h and c_h and the functional f_h are given by

$$\begin{aligned}
a_h(\boldsymbol{u}, \boldsymbol{v}) &= \int_\Omega \mu^{-1} \nabla_h \times \boldsymbol{u} \cdot \nabla_h \times \boldsymbol{v} \, d\boldsymbol{x} - \int_{\mathcal{F}_h} [\![\boldsymbol{u}]\!]_T \cdot \{\!\{\mu^{-1} \nabla_h \times \boldsymbol{v}\}\!\} \, ds \\
&\quad - \int_{\mathcal{F}_h} [\![\boldsymbol{v}]\!]_T \cdot \{\!\{\mu^{-1} \nabla_h \times \boldsymbol{u}\}\!\} \, ds + \int_{\mathcal{F}_h} \mathtt{a} \, [\![\boldsymbol{u}]\!]_T \cdot [\![\boldsymbol{v}]\!]_T \, ds \\
&\quad + \int_{\mathcal{F}_h^{\mathcal{I}}} \mathtt{b} \, [\![\varepsilon \boldsymbol{u}]\!]_N [\![\varepsilon \boldsymbol{v}]\!]_N \, ds, \\
b_h(\boldsymbol{v}, p) &= - \int_\Omega \varepsilon \boldsymbol{v} \cdot \nabla_h p \, d\boldsymbol{x} + \int_{\mathcal{F}_h} \{\!\{\varepsilon \boldsymbol{v}\}\!\} \cdot [\![p]\!]_N \, ds, \\
c_h(p, q) &= \int_{\mathcal{F}_h} \mathtt{c} [\![p]\!]_N \cdot [\![q]\!]_N \, ds, \\
f_h(\boldsymbol{v}) &= \int_\Omega \boldsymbol{j} \cdot \boldsymbol{v} \, d\boldsymbol{x} - \int_{\mathcal{F}_h^{\mathcal{D}}} \boldsymbol{g} \cdot \mu^{-1} \nabla_h \times \boldsymbol{v} \, ds + \int_{\mathcal{F}_h^{\mathcal{D}}} \mathtt{a} \boldsymbol{g} \cdot (\boldsymbol{n} \times \boldsymbol{v}) \, ds,
\end{aligned}$$

respectively. Here, ∇_h denotes the elementwise ∇ operator. The form a_h corresponds to the interior penalty discretization of the curl-curl operator [25, 19], with the addition of a normal jump term, the form b_h discretizes the divergence operator in a DG fashion (see, e.g., [11, 18, 29, 28] and the reference cited therein for related DG approaches for the Stokes system and linear elasticity problems), and the form c_h is a stabilization form that penalizes the jumps of p_h. The parameters $\mathtt{a}$, $\mathtt{b}$ and $\mathtt{c}$ are positive stabilization parameters that will be chosen later on, depending on the mesh size and the coefficients μ and ε. Note that a similar discretization has been investigated in [25] for a time-harmonic high-frequency model of Maxwell's equations; we point out that the additional stabilization forms that have been added there become obsolete with the analysis presented in this paper.

REMARK 2.2. *For test functions $(\boldsymbol{v}, q) \in \boldsymbol{V}_h \times Q_h$, integration by parts gives*

$$b_h(\boldsymbol{v}, q) = \int_\Omega q \, \nabla_h \cdot (\varepsilon \boldsymbol{v}) \, d\boldsymbol{x} - \int_{\mathcal{F}_h^{\mathcal{I}}} \{\!\{q\}\!\} \, [\![\varepsilon \boldsymbol{v}]\!]_N \, ds.$$

REMARK 2.3. *By noting that the exact solution $(\boldsymbol{u}, p)$ of problem (2.1) satisfies $\boldsymbol{u} \in H_0(\mathrm{curl}; \Omega) \cap H(\mathrm{div}_\varepsilon^0; \Omega)$, $\mu^{-1} \nabla \times \boldsymbol{u} \in H(\mathrm{curl}; \Omega)$ and $p \in H_0^1(\Omega)$, and by using the same arguments as in [24, Remark 3.2] or [25, Proposition 4], it can be seen that the method (2.5)–(2.6) is consistent. That is, the exact solution $(\boldsymbol{u}, p) \in \boldsymbol{V} \times Q$ satisfies the equations (2.5)–(2.6) for all test functions $(\boldsymbol{v}, q) \in \boldsymbol{V}_h \times Q_h$.*

PROPOSITION 2.4. *For positive stabilization parameters* a, b *and* c, *the mixed DG method (2.5)–(2.6) has a unique solution.*

Proof. Due to the linearity and finite-dimensionality of the problem, it is enough to show that $\boldsymbol{j} = \mathbf{0}$ and $\boldsymbol{g} = \mathbf{0}$ imply $\boldsymbol{u}_h = \mathbf{0}$ and $p_h = 0$. To this end, take $\boldsymbol{v} = \boldsymbol{u}_h$ in (2.5) and $q = p_h$ in (2.6), then subtract (2.6) from (2.5). It follows that $\nabla_h \times \boldsymbol{u}_h = \mathbf{0}$, $[\![\boldsymbol{u}_h]\!]_T = \mathbf{0}$ on $\mathcal{F}_h$, $[\![\varepsilon \boldsymbol{u}_h]\!]_N = 0$ on $\mathcal{F}_h^{\mathcal{I}}$, and $[\![p]\!]_N = \mathbf{0}$ on $\mathcal{F}_h$, i.e., $\boldsymbol{u}_h \in H_0(\mathrm{curl}^0;\Omega) \cap H(\mathrm{div}_\varepsilon;\Omega)$ and $p \in H^1_0(\Omega)$. Equation (2.6) thus becomes $\int_\Omega q \nabla \cdot (\varepsilon \boldsymbol{u}_h)\, d\boldsymbol{x} = 0$, for any $q \in Q_h$, and then, since ε is piecewise constant, $\nabla \cdot (\varepsilon \boldsymbol{u}_h) = 0$. Therefore, $\boldsymbol{u}_h \in H_0(\mathrm{curl}^0;\Omega) \cap H(\mathrm{div}^0_\varepsilon;\Omega)$, which, owing to our assumptions on Ω, implies that $\boldsymbol{u}_h = \mathbf{0}$; cf. [17, Section 4]. Equation (2.5) becomes $\int_\Omega \varepsilon \boldsymbol{v} \cdot \nabla p_h \, d\boldsymbol{x} = 0$, for any $\boldsymbol{v} \in V_h$, and then $\nabla p_h = \mathbf{0}$. This, together with $p_h = 0$ on Γ, gives that $p_h = 0$. ☐

REMARK 2.5. *Several other DG discretizations can be used for the form* a_h; *we mention here only the non-symmetric interior penalty form (see, e.g., [4, 20, 27, 26] in the context of diffusion problems or [19, 25] in the context of Maxwell's equations), or the local discontinuous Galerkin form used in [24]. The setting that we present here applies to these forms too and the error bounds that we obtain hold verbatim for these methods as well.*

REMARK 2.6. *All the interface contributions in the forms in (2.5)–(2.6) can be easily obtained by rewriting the problem (2.1) as a first-order system and by introducing the so-called* numerical fluxes *in the sense of [4]. Thus, all the stabilization terms in (2.5)–(2.6) are* local, consistent *and* conservative. *To see this, we rewrite (2.1) as*

$$\begin{aligned} \boldsymbol{s} - \mu^{-1}\nabla \times \boldsymbol{u} &= 0 && \text{in } \Omega, \\ \nabla \times \boldsymbol{s} - \varepsilon \nabla p &= \boldsymbol{j} && \text{in } \Omega, \\ \nabla \cdot (\varepsilon \boldsymbol{u}) &= 0 && \text{in } \Omega, \\ \boldsymbol{n} \times \boldsymbol{u} &= \boldsymbol{g} && \text{on } \Gamma, \\ p &= 0 && \text{on } \Gamma; \end{aligned}$$

then we consider the following discretization: find $(\boldsymbol{s}_h, \boldsymbol{u}_h, p_h) \in \boldsymbol{V}_h \times \boldsymbol{V}_h \times Q_h$ *such that*

$$\begin{aligned} &\int_K \boldsymbol{s}_h \cdot \boldsymbol{t}\, d\boldsymbol{x} - \int_K \mu^{-1}\nabla \times \boldsymbol{t} \cdot \boldsymbol{u}_h \, d\boldsymbol{x} + \int_{\partial K} \mu^{-1}\boldsymbol{t} \cdot \widehat{\boldsymbol{u}}_h \times \boldsymbol{n}\, ds = 0, \\ &\int_K \boldsymbol{s}_h \cdot \nabla \times \boldsymbol{v}\, d\boldsymbol{x} - \int_{\partial K} \boldsymbol{v} \cdot \widehat{\boldsymbol{s}}_h \times \boldsymbol{n}\, ds + \int_K p_h \nabla \cdot (\varepsilon \boldsymbol{v})\, d\boldsymbol{x} \\ &\qquad\qquad - \int_{\partial K} \widehat{p}_h\, \varepsilon \boldsymbol{v} \cdot \boldsymbol{n}\, ds = \int_K \boldsymbol{j} \cdot \boldsymbol{v}\, d\boldsymbol{x}, \\ &\int_K \varepsilon \boldsymbol{u}_h \cdot \nabla q\, d\boldsymbol{x} - \int_{\partial K} q\, \widehat{\varepsilon \boldsymbol{u}}_h \cdot \boldsymbol{n}\, ds = 0 \end{aligned} \tag{2.7}$$

for all $(\boldsymbol{t}, \boldsymbol{v}, q) \in \boldsymbol{V}_h \times \boldsymbol{V}_h \times Q_h$, *and for all elements* K *in the partition* $\mathcal{T}_h$. *In (2.7), the traces of* $\boldsymbol{u}$, $\boldsymbol{s}$, p *and* $\varepsilon \boldsymbol{u}$ *on* ∂K *are approximated by the numerical fluxes*

$$\begin{aligned} \widehat{\boldsymbol{u}}_h &= \{\!\{\boldsymbol{u}_h\}\!\}, & \widehat{\boldsymbol{s}}_h &= \{\!\{\mu^{-1}\nabla_h \times \boldsymbol{u}_h\}\!\} - \mathsf{a}[\![\boldsymbol{u}_h]\!]_T, \\ \widehat{p}_h &= \{\!\{p_h\}\!\} - \mathsf{b}[\![\varepsilon \boldsymbol{u}_h]\!]_N, & \widehat{\varepsilon \boldsymbol{u}}_h &= \{\!\{\varepsilon \boldsymbol{u}_h\}\!\} - \mathsf{c}[\![p_h]\!]_N, \end{aligned}$$

respectively, (these definitions are for interior faces; they must be suitably adapted on boundary faces). The auxiliary variable $\boldsymbol{s}_h$ *can then be eliminated from (2.7), giving rise to an elemental formulation in the unknowns* $\boldsymbol{u}_h$ *and* p_h *only. Finally, summing over all* $K \in \mathcal{T}_h$ *gives the formulation (2.5)–(2.6). We refer to [4] and [24] for further details.*

3. Main results. In this section, we state a priori error estimates for the mixed DG method in (2.5)–(2.6). The proofs of these results will be given in Sections 4, 5 and 6.

3.1. Stabilization parameters and DG-norms. We start by defining the stabilization parameters $\mathtt{a}$, $\mathtt{b}$ and $\mathtt{c}$ appearing in (2.5)–(2.6) and introduce the norms employed in the proceeding error analysis.

To this end, we first define the function $\mathtt{h}$ in $L^\infty(\mathcal{F}_h)$, representing the local mesh size, as

$$\mathtt{h}(\boldsymbol{x}) = \begin{cases} \min\{h_K, h_{K'}\} & \text{if } \boldsymbol{x} \text{ is in the interior of } \partial K \cap \partial K', \\ h_K & \text{if } \boldsymbol{x} \text{ is in the interior of } \partial K \cap \Gamma, \end{cases}$$

where K and K' are two neighboring elements in the mesh $\mathcal{T}_h$. Similarly, we define the functions $\mathtt{m}$ and $\mathtt{e}$ in $L^\infty(\mathcal{F}_h)$ by $\mathtt{m}(\boldsymbol{x}) = \min\{\mu_K, \mu_{K'}\}$ and $\mathtt{e}(\boldsymbol{x}) = \max\{\varepsilon_K, \varepsilon_{K'}\}$, if $\boldsymbol{x}$ is in the interior of $\partial K \cap \partial K'$, and $\mathtt{m}(\boldsymbol{x}) = \mu_K$ and $\mathtt{e}(\boldsymbol{x}) = \varepsilon_K$, if $\boldsymbol{x}$ is in the interior of $\partial K \cap \Gamma$, with μ_K and ε_K denoting the restrictions of μ and ε to the element K, respectively (recall that μ and ε are constant within each element).

With this notation, we choose the stabilization parameters as follows:

$$\mathtt{a} = \alpha\, \mathtt{m}^{-1}\mathtt{h}^{-1}, \qquad \mathtt{b} = \beta\, \mathtt{e}^{-1}\mathtt{h}, \qquad \mathtt{c} = \gamma\, \mathtt{e}\mathtt{h}^{-1}, \tag{3.1}$$

where α, β and γ are positive parameters independent of the mesh size and the coefficients μ and ε.

Next, we define the spaces

$$\boldsymbol{V}(h) = (\boldsymbol{V} \cap H(\mathrm{div}_\varepsilon; \Omega)) + \boldsymbol{V}_h, \qquad Q(h) = Q + Q_h,$$

and the following DG-seminorm and DG-norms, respectively:

$$\begin{aligned} |\boldsymbol{v}|^2_{\boldsymbol{V}(h)} &= \|\mu^{-\frac{1}{2}} \nabla_h \times \boldsymbol{v}\|^2_{0,\Omega} + \|\mathtt{m}^{-\frac{1}{2}}\mathtt{h}^{-\frac{1}{2}} [\![\boldsymbol{v}]\!]_T\|^2_{0,\mathcal{F}_h} + \|\mathtt{e}^{-\frac{1}{2}}\mathtt{h}^{\frac{1}{2}} [\![\varepsilon \boldsymbol{v}]\!]_N\|^2_{0,\mathcal{F}_h^{\mathcal{I}}}, \\ \|\boldsymbol{v}\|^2_{\boldsymbol{V}(h)} &= \|\varepsilon^{\frac{1}{2}} \boldsymbol{v}\|^2_{0,\Omega} + |\boldsymbol{v}|^2_{\boldsymbol{V}(h)}, \\ \|q\|^2_{Q(h)} &= \|\varepsilon^{\frac{1}{2}} \nabla_h q\|^2_{0,\Omega} + \|\mathtt{e}^{\frac{1}{2}}\mathtt{h}^{-\frac{1}{2}} [\![q]\!]_N\|^2_{0,\mathcal{F}_h}. \end{aligned}$$

Finally, we introduce the broken Sobolev space

$$H^s(\mathcal{T}_h) = \{\, v \in L^2(\Omega) : \ v|_K \in H^s(K), \ K \in \mathcal{T}_h \,\},$$

endowed with the norm $\|v\|^2_{s,\mathcal{T}_h} = \sum_{K \in \mathcal{T}_h} \|v\|^2_{s,K}$. On the boundary, we write

$$H^s(\mathcal{F}_h^{\mathcal{D}}) = \{\, v \in L^2(\mathcal{F}_h^{\mathcal{D}}) : \ v|_f \in H^s(f), \ f \subset \mathcal{F}_h^{\mathcal{D}} \,\},$$

equipped with the norm $\|v\|^2_{s,\mathcal{F}_h^{\mathcal{D}}} = \sum_{f \subset \mathcal{F}_h^{\mathcal{D}}} \|v\|^2_{s,f}$. Since the boundary datum $\boldsymbol{g}$ is the tangential trace on Γ of a function in $H(\mathrm{curl}; \Omega)$, its restriction to each $f \subset \mathcal{F}_h^{\mathcal{D}}$ is a two-dimensional vector field which lies on the same plane as f. Hence, we can understand $\boldsymbol{g}$ as a function in $L^2(\Gamma)^2$.

3.2. A priori error estimates. First, we establish optimal error estimates for smooth solutions on possibly nonconforming meshes subject to the following restrictions:

(i) any interior face $f \subset \mathcal{F}_h^{\mathcal{I}}$ has to be an *entire* elemental face of at least one of the two adjacent elements sharing f;

(ii) the number of interior faces contained in an elemental face is uniformly bounded with respect to the mesh size h.

This implies bounded variation of the local mesh size, i.e., whenever K and K' share a common face and $h_K \geq h_{K'}$,

$$h_K \leq C h_{K'} \leq C h_K, \tag{3.2}$$

for a constant $C > 0$ independent of the mesh size. The reason for this restriction is related to the validity of the norm-equivalence result of Theorem 5.5 below.

Our first main result establishes optimal convergence of the error in the DG–norm.

THEOREM 3.1. *Let $(\boldsymbol{u}, p)$ be the exact solution of (2.1) satisfying*

$$\boldsymbol{u} \in H^{s+1}(\mathcal{T}_h)^3, \qquad p \in H^{s+1}(\mathcal{T}_h), \tag{3.3}$$

for a regularity exponent $s > \frac{1}{2}$. Let $(\boldsymbol{u}_h, p_h)$ be the mixed DG approximation obtained by (2.5)–(2.6) on possibly nonconforming meshes that satisfy the restrictions (i) and (ii) above. Then we have the a priori error bound

$$\|\boldsymbol{u} - \boldsymbol{u}_h\|_{\boldsymbol{V}(h)} + \|p - p_h\|_{Q(h)} \leq C\, h^{\min\{s,\ell\}} \Big[\|\boldsymbol{u}\|_{s+1,\mathcal{T}_h} + \|p\|_{s+1,\mathcal{T}_h} \Big],$$

with a constant $C > 0$ depending on the bounds (2.2) on the coefficients μ and ε, the shape-regularity of the mesh, the constant in (3.2), the stabilization parameters α, β and γ, and the polynomial degree ℓ, but independent of the mesh size h.

While the bounds in Theorem 3.1 guarantee optimal convergence in the mesh size h with respect to the polynomial degree used in the approximation, the smoothness assumptions (3.3) on the exact solution are not minimal. In fact, for $\varepsilon = \mu = 1$ and a homogeneous Dirichlet datum $\boldsymbol{g} \equiv \boldsymbol{0}$, from the regularity results in [3], it follows that, on general polyhedral domains, one only has $\boldsymbol{u} \in H^s(\Omega)^3$ and $\nabla \times \boldsymbol{u} \in H^s(\Omega)^3$, for a regularity exponent $s = s(\Omega) > \frac{1}{2}$ (the same actually holds true for smooth coefficients ε and μ; see [25, Section 2.2]). As far as the assumption $p \in H^{s+1}(\Omega)$ is concerned, although it does not seem to hold true for general source terms $\boldsymbol{j}$ in $L^2(\Omega)^3$, it is trivially satisfied in the physically most relevant case of divergence-free source terms $\boldsymbol{j}$, where $p \equiv 0$.

For these reasons, we state a second result under weaker smoothness assumptions for the component $\boldsymbol{u}$ of the exact solution. In order to do this, we restrict ourselves to the case of conforming meshes (i.e., meshes with no hanging nodes); this restriction is necessary, since the proof requires the use of $H(\mathrm{curl};\Omega)$–conforming projectors.

THEOREM 3.2. *Let $(\boldsymbol{u}, p)$ be the exact solution of (2.1) satisfying*

$$\varepsilon \boldsymbol{u} \in H^s(\mathcal{T}_h)^3, \quad \mu^{-1}\nabla \times \boldsymbol{u} \in H^s(\mathcal{T}_h)^3, \quad p \in H^{s+1}(\mathcal{T}_h), \quad \boldsymbol{g} \in H^{s+\frac{1}{2}}(\mathcal{F}_h^{\mathcal{D}})^2,$$

for a regularity exponent $s > \frac{1}{2}$. Let $(\boldsymbol{u}_h, p_h)$ be the mixed DG approximation obtained by (2.5)–(2.6) on conforming meshes. Then we have the a priori error bound

$$\begin{aligned} &\|\boldsymbol{u} - \boldsymbol{u}_h\|_{\boldsymbol{V}(h)} + \|p - p_h\|_{Q(h)} \\ &\quad \leq C\, h^{\min\{s,\ell\}} \Big[\|\varepsilon \boldsymbol{u}\|_{s,\mathcal{T}_h} + \|\mu^{-1}\nabla \times \boldsymbol{u}\|_{s,\mathcal{T}_h} + \|p\|_{s+1,\mathcal{T}_h} + \|\boldsymbol{g}\|_{s+\frac{1}{2},\mathcal{F}_h^{\mathcal{D}}} \Big], \end{aligned}$$

with a constant $C > 0$ depending on the bounds (2.2) on the coefficients μ and ε, the shape-regularity of the mesh, the stabilization parameters α, β and γ, and the polynomial degree ℓ, but independent of the mesh size h.

REMARK 3.3. *The numerical results reported in Section 7 show that, on a two-dimensional L-shaped domain, the above convergence rates are obtained also on highly distorted and nonconforming meshes for the strongest corner singularities.*

The mixed method in (2.5)–(2.6) enforces the divergence constraint in a weak sense only. Nevertheless, the convergence rate of the error in the actual (elementwise) divergence might be of interest. Our last result addresses this issue and proves a rate that is of one order lower than the error measured in the DG–norm. This result is numerically observed to be sharp on conforming finite element meshes, cf. Section 7.

THEOREM 3.4. *Let $(\boldsymbol{u}, p)$ be the exact solution of (2.1) and $(\boldsymbol{u}_h, p_h)$ be the mixed DG approximation obtained by (2.5)–(2.6) on a possibly nonconforming mesh satisfying the restrictions (i) and (ii) above. Then we have*

$$\sum_{K\in\mathcal{T}_h} h_K^2 \|\nabla\cdot(\varepsilon(\boldsymbol{u}-\boldsymbol{u}_h))\|_{0,K}^2 \leq C\left[\|\mathrm{h}^{\frac{1}{2}}[\![\varepsilon\boldsymbol{u}-\varepsilon\boldsymbol{u}_h]\!]_N\|_{\mathcal{F}_h^{\mathcal{I}}}^2 + \|\mathrm{e}^{\frac{1}{2}}\mathrm{h}^{-\frac{1}{2}}[\![q-q_h]\!]_N\|_{0,\mathcal{F}_h}^2\right],$$

with a constant $C > 0$ depending on the shape-regularity of the mesh, the constant in (3.2), the stabilization parameter γ, and the polynomial degree ℓ, but independent of the mesh size h.

REMARK 3.5. *In both of the cases of Theorem 3.1 and Theorem 3.2, the estimate in Theorem 3.4 implies that*

$$\Big[\sum_{K\in\mathcal{T}_h} h_K^2 \|\nabla\cdot(\varepsilon(\boldsymbol{u}-\boldsymbol{u}_h))\|_{0,K}^2\Big]^{\frac{1}{2}} \leq C\, h^{\min\{s,\ell\}},$$

with a constant $C > 0$ independent of the mesh size.

The proofs of Theorems 3.1, 3.2 and 3.4 are carried out in the next sections and concluded in Sections 6.2 and 6.3.

4. Auxiliary mixed formulation. In order to facilitate the error analysis, we rewrite the discrete formulation (2.5)–(2.6) in a different (and nonconforming) form, by introducing the jumps of p_h as auxiliary unknowns and by employing lifting operators as in [4, 24]. In this way, the resulting bilinear forms have suitable continuity and coercivity properties, so that the method can be analyzed by using the classical theory of mixed finite methods.

We begin by introducing the lifting operators $\mathcal{L}$ and $\mathcal{M}$. For $\boldsymbol{v}$ belonging to $\boldsymbol{V}(h)$, we define $\mathcal{L}(\boldsymbol{v}) \in \boldsymbol{V}_h$ by

$$\int_\Omega \mathcal{L}(\boldsymbol{v})\cdot\boldsymbol{w}\,d\boldsymbol{x} = \int_{\mathcal{F}_h} [\![\boldsymbol{v}]\!]_T\cdot\{\!\{\boldsymbol{w}\}\!\}\,ds \qquad \forall \boldsymbol{w}\in\boldsymbol{V}_h, \tag{4.1}$$

and, for q in $Q(h)$, we define $\mathcal{M}(q) \in \boldsymbol{V}_h$ by

$$\int_\Omega \mathcal{M}(q)\cdot\boldsymbol{w}\,d\boldsymbol{x} = \int_{\mathcal{F}_h} \{\!\{\boldsymbol{w}\}\!\}\cdot[\![q]\!]_N\,ds \qquad \forall \boldsymbol{w}\in\boldsymbol{V}_h. \tag{4.2}$$

We now define the forms

$$\begin{aligned}
\widetilde{a}_h(\boldsymbol{u},\boldsymbol{v}) = &\int_\Omega \mu^{-1}\nabla_h \times \boldsymbol{u}\cdot\nabla_h\times\boldsymbol{v}\,d\boldsymbol{x} - \int_\Omega \mathcal{L}(\boldsymbol{u})\cdot(\mu^{-1}\nabla_h\times\boldsymbol{v})\,d\boldsymbol{x}\\
&- \int_\Omega \mathcal{L}(\boldsymbol{v})\cdot(\mu^{-1}\nabla_h\times\boldsymbol{u})\,d\boldsymbol{x} + \int_{\mathcal{F}_h} \mathsf{a}\,[\![\boldsymbol{u}]\!]_T\cdot[\![\boldsymbol{v}]\!]_T\,ds\\
&+ \int_{\mathcal{F}_h^{\mathcal{I}}} \mathsf{b}\,[\![\varepsilon\boldsymbol{u}]\!]_N[\![\varepsilon\boldsymbol{v}]\!]_N\,ds,\\
\widetilde{b}_h(\boldsymbol{v},p) = &-\int_\Omega \varepsilon\boldsymbol{v}\cdot\left[\nabla_h p - \mathcal{M}(p)\right]d\boldsymbol{x}.
\end{aligned}$$

Note that $a_h = \widetilde{a}_h$ in $\boldsymbol{V}_h\times\boldsymbol{V}_h$ and $b_h = \widetilde{b}_h$ in $\boldsymbol{V}_h\times Q_h$, although this is no longer true in $\boldsymbol{V}(h)\times\boldsymbol{V}(h)$ and in $\boldsymbol{V}(h)\times Q(h)$, respectively.

Next, we define the discrete space

$$M_h = \{\lambda\in L^2(\mathcal{F}_h) : \lambda|_f \in \mathcal{S}^\ell(f) \quad \forall f\subset\mathcal{F}_h\},$$

endowed with the norm $\|\eta\|_{M_h} = \|\mathsf{e}^{\frac{1}{2}}\mathsf{h}^{-\frac{1}{2}}\eta\|_{0,\mathcal{F}_h}$, and consider the following auxiliary mixed formulation: find $(\boldsymbol{u}_h,\lambda_h,p_h)\in\boldsymbol{V}_h\times M_h\times Q_h$ such that

$$\begin{aligned}
A_h(\boldsymbol{u}_h,\lambda_h;\boldsymbol{v},\eta) + B_h(\boldsymbol{v},\eta;p_h) &= f_h(\boldsymbol{v}) \qquad \forall(\boldsymbol{v},\eta)\in\boldsymbol{V}_h\times M_h, &(4.3)\\
B_h(\boldsymbol{u}_h,\lambda_h;q) &= 0 \qquad \forall q\in Q_h, &(4.4)
\end{aligned}$$

with forms A_h and B_h given by

$$\begin{aligned}
A_h(\boldsymbol{u},\lambda;\boldsymbol{v},\eta) &= \widetilde{a}_h(\boldsymbol{u},\boldsymbol{v}) + \int_{\mathcal{F}_h} \mathsf{c}\lambda\eta\,ds,\\
B_h(\boldsymbol{v},\eta;p) &= \widetilde{b}_h(\boldsymbol{v},p) - \int_{\mathcal{F}_h} \mathsf{c}[\![p]\!]_N\eta\,ds.
\end{aligned} \tag{4.5}$$

PROPOSITION 4.1. *Problem (4.3)–(4.4) admits a unique solution* $(\boldsymbol{u}_h,\lambda_h,p_h)\in\boldsymbol{V}_h\times M_h\times Q_h$, *with* $(\boldsymbol{u}_h,p_h)$ *the solution to (2.5)–(2.6), and* $\lambda_h = [\![p_h]\!]_N$.

Proof. By choosing test functions $(\boldsymbol{0},\eta)$ in (4.3), we have

$$\int_{\mathcal{F}_h} \mathsf{c}\lambda_h\eta\,ds = \int_{\mathcal{F}_h} \mathsf{c}[\![p_h]\!]_N\eta\,ds \qquad \forall\eta\in M_h.$$

Since c is constant on each $f\in\mathcal{F}_h$, we have that $\lambda_h = [\![p_h]\!]_N$. Then, equations (4.3) and (4.4) coincide with equations (2.5) and (2.6), respectively. Therefore, if $(\boldsymbol{u}_h,\lambda_h,p_h)\in\boldsymbol{V}_h\times M_h\times Q_h$ is a solution to (4.3)–(4.4), then $\lambda_h = [\![p_h]\!]_N$ and $(\boldsymbol{u}_h,p_h)$ is (the unique) solution to (2.5)–(2.6), which proves uniqueness of the solution. Existence follows from uniqueness. □

Finally, we introduce the space $\boldsymbol{W}(h) = \boldsymbol{V}(h)\times M_h$ and the product seminorm and norm

$$|(\boldsymbol{v},\eta)|^2_{\boldsymbol{W}(h)} = |\boldsymbol{v}|^2_{\boldsymbol{V}(h)} + \|\eta\|^2_{M_h}, \qquad \|(\boldsymbol{v},\eta)\|^2_{\boldsymbol{W}(h)} = \|\boldsymbol{v}\|^2_{\boldsymbol{V}(h)} + \|\eta\|^2_{M_h},$$

respectively, which will be employed in the following analysis.

The proofs of Theorems 3.1, 3.2 and 3.4 are now carried out by analyzing the auxiliary mixed formulation (4.3)–(4.4). In Section 5 we prove the continuity of A_h and B_h, the ellipticity of A_h on the kernel of B_h, as well as the inf-sup condition for B_h. In the proof of the inf-sup condition, we make use of a crucial norm-equivalence property whose detailed derivation can be found in the appendix. Then, the error estimates of Theorems 3.1, 3.2 and 3.4 are obtained in Section 6.

5. Continuity and stability. In this section, we prove continuity properties of the forms A_h and B_h, the ellipticity of A_h on the kernel of B_h, as well as the inf-sup condition for B_h.

5.1. Continuity properties. We begin by noting the following stability properties for the lifting operators $\mathcal{L}$ and $\mathcal{M}$:

$$\|\mu^{-\frac{1}{2}}\mathcal{L}(\boldsymbol{v})\|_{0,\Omega} \leq C_{\text{lift}}\|\mathtt{m}^{-\frac{1}{2}}\mathtt{h}^{-\frac{1}{2}}[\![\boldsymbol{v}]\!]_T\|_{0,\mathcal{F}_h}, \quad \|\varepsilon^{\frac{1}{2}}\mathcal{M}(q)\|_{0,\Omega} \leq C_{\text{lift}}\|\mathtt{e}^{\frac{1}{2}}\mathtt{h}^{-\frac{1}{2}}[\![q]\!]_N\|_{0,\mathcal{F}_h}, \tag{5.1}$$

with a constant $C_{\text{lift}} > 0$ that is independent of the mesh size and the coefficients μ and ε. This can been seen by using the same arguments as in [24, Proposition 4.2] or [25, Proposition 12]. Similarly, by defining the lifting operator $\boldsymbol{G}_{\mathcal{D}} \in \boldsymbol{V}_h$ of the boundary datum by $\int_\Omega \boldsymbol{G}_{\mathcal{D}} \cdot \boldsymbol{w}\, d\boldsymbol{x} = \int_\Gamma \boldsymbol{g} \cdot \boldsymbol{w}\, ds$ for all $\boldsymbol{w} \in \boldsymbol{V}_h$, we have

$$\|\mu^{-\frac{1}{2}}\boldsymbol{G}_{\mathcal{D}}\|_{0,\Omega} \leq C_{\text{lift}}\|\mathtt{m}^{-\frac{1}{2}}\mathtt{h}^{-\frac{1}{2}}\boldsymbol{g}\|_{0,\Gamma}. \tag{5.2}$$

The following continuity properties hold true.

PROPOSITION 5.1. *The forms $A_h : \boldsymbol{W}(h) \times \boldsymbol{W}(h) \to \mathbb{R}$ and $B_h : \boldsymbol{W}(h) \times Q(h) \to \mathbb{R}$ are continuous, i.e., there exist constants $a_1 > 0$ and $a_2 > 0$ independent of the mesh size and the coefficients μ and ε, such that, for any $(\boldsymbol{u}, \lambda), (\boldsymbol{v}, \eta) \in \boldsymbol{W}(h)$ and $q \in Q(h)$,*

$$\begin{aligned} |A_h(\boldsymbol{u}, \lambda; \boldsymbol{v}, \eta)| &\leq a_1 \,\|(\boldsymbol{u}, \lambda)\|_{\boldsymbol{W}(h)}\|(\boldsymbol{v}, \eta)\|_{\boldsymbol{W}(h)}, \\ |B_h(\boldsymbol{v}, \eta; q)| &\leq a_2 \,\|(\boldsymbol{v}, \eta)\|_{\boldsymbol{W}(h)}\|q\|_{Q(h)}. \end{aligned}$$

The linear functional $f_h : \boldsymbol{V}_h \to \mathbb{R}$ on the right-hand side of (4.3) is continuous and satisfies

$$|f_h(\boldsymbol{v})| \leq C\big[\varepsilon_*^{-\frac{1}{2}}\|\boldsymbol{j}\|_{0,\Omega} + \|\mathtt{m}^{-\frac{1}{2}}\mathtt{h}^{-\frac{1}{2}}\boldsymbol{g}\|_{0,\Gamma}^2\big]\,\|\boldsymbol{v}\|_{\boldsymbol{V}(h)},$$

with a constant $C > 0$ independent of the mesh size and the coefficients μ and ε.

Proof. The continuity properties of A_h and B_h follow as a consequence of the estimates in (5.1) and the choice of the stabilization parameters, cf. (3.1). From the definition of a and the lifting operator $\boldsymbol{G}_{\mathcal{D}}$, the bounds in (2.2), the Cauchy-Schwarz inequality, and the definition of the $\boldsymbol{V}(h)$–norm, we have

$$|f_h(\boldsymbol{v})| \leq C\big[\varepsilon_*^{-\frac{1}{2}}\|\boldsymbol{j}\|_{0,\Omega} + \|\mu^{-\frac{1}{2}}\boldsymbol{G}_{\mathcal{D}}\|_{0,\Omega} + \|\mathtt{m}^{-\frac{1}{2}}\mathtt{h}^{-\frac{1}{2}}\boldsymbol{g}\|_{0,\Gamma}^2\big]\,\|\boldsymbol{v}\|_{\boldsymbol{V}(h)},$$

for any $\boldsymbol{v} \in \boldsymbol{V}_h$. Then, the continuity property of f_h follows from (5.2). ◻

5.2. Ellipticity on the kernel. Define the discrete kernel

$$\text{Ker}(B_h) = \{(\boldsymbol{u}, \lambda) \in \boldsymbol{W}_h : B_h(\boldsymbol{u}, \lambda; p) = 0 \;\forall p \in Q_h\}.$$

We now establish the following coercivity property.

PROPOSITION 5.2. *There exists a parameter $\alpha_{\min} > 0$, independent of the mesh size and the coefficients μ and ε, such that, for all stabilization parameters $\alpha \geq \alpha_{\min}$, $\beta > 0$, $\gamma > 0$, there exists a constant $b > 0$ independent of the mesh size such that, for any $(\boldsymbol{u}, \lambda) \in \text{Ker}(B_h)$,*

$$A_h(\boldsymbol{u}, \lambda; \boldsymbol{u}, \lambda) \geq b\,\|(\boldsymbol{u}, \lambda)\|_{\boldsymbol{W}(h)}^2.$$

REMARK 5.3. *The condition $\alpha \geq \alpha_{\min} > 0$ is a restriction that is typically encountered in symmetric interior penalty methods. For other DG discretizations of the curl-curl operator, such as the non-symmetric interior penalty or the LDG method, stability is guaranteed for any stabilization parameter $\alpha > 0$; see, e.g., [4, 19, 24] for details.*

REMARK 5.4. *In general, as for the continuous problem, the ellipticity constant b depends on the bounds (2.2) of μ and ε in a rather complicated manner that we do not make explicit.*

Proof of Proposition 5.2. For α large enough, we have

$$A_h(\boldsymbol{u},\lambda;\boldsymbol{u},\lambda) \geq C\,|(\boldsymbol{u},\lambda)|^2_{\boldsymbol{W}(h)}, \tag{5.3}$$

for any $(\boldsymbol{u},\lambda) \in \boldsymbol{W}_h$, with a constant C independent of the mesh size and the coefficients μ and ε. In fact,

$$\begin{aligned}
A_h(\boldsymbol{u},\lambda;\boldsymbol{u},\lambda) =& \|\mu^{-\frac12}\nabla_h\times\boldsymbol{u}\|^2_{0,\Omega} - 2\int_\Omega \mathcal{L}(\boldsymbol{u})\cdot\mu^{-1}\nabla_h\times\boldsymbol{u}\,d\boldsymbol{x}\\
&+\alpha\|\mathtt{m}^{-\frac12}\mathtt{h}^{-\frac12}[\![\boldsymbol{u}]\!]_T\|^2_{0,\mathcal{F}_h} + \beta\|\mathtt{e}^{-\frac12}\mathtt{h}^{\frac12}[\![\varepsilon\boldsymbol{u}]\!]_N\|^2_{0,\mathcal{F}_h^{\mathcal{I}}} + \gamma\|\lambda\|^2_{M_h}\\
\geq& \|\mu^{-\frac12}\nabla_h\times\boldsymbol{u}\|^2_{0,\Omega} - \delta\|\mu^{-\frac12}\mathcal{L}(\boldsymbol{u})\|^2_{0,\Omega} - \delta^{-1}\|\mu^{-\frac12}\nabla_h\times\boldsymbol{u}\|^2_{0,\Omega}\\
&+\alpha\|\mathtt{m}^{-\frac12}\mathtt{h}^{-\frac12}[\![\boldsymbol{u}]\!]_T\|^2_{0,\mathcal{F}_h} + \beta\|\mathtt{e}^{-\frac12}\mathtt{h}^{\frac12}[\![\varepsilon\boldsymbol{u}]\!]_N\|^2_{0,\mathcal{F}_h^{\mathcal{I}}} + \gamma\|\lambda\|^2_{M_h}\\
\geq& (1-\delta^{-1})\|\mu^{-\frac12}\nabla_h\times\boldsymbol{u}\|^2_{0,\Omega} + (\alpha-\delta\,C^2_{\rm lift})\|\mathtt{m}^{-\frac12}\mathtt{h}^{-\frac12}[\![\boldsymbol{u}]\!]_T\|^2_{0,\mathcal{F}_h}\\
&+\beta\|\mathtt{e}^{-\frac12}\mathtt{h}^{\frac12}[\![\varepsilon\boldsymbol{u}]\!]_N\|^2_{0,\mathcal{F}_h^{\mathcal{I}}} + \gamma\|\lambda\|^2_{M_h},
\end{aligned}$$

where $C_{\rm lift}$ is the constant in (5.1), and δ is a positive constant still at our disposal. Therefore, provided that $\alpha > \alpha_{\min} = C^2_{\rm lift}$, we can choose δ satisfying $1 < \delta < \alpha/C^2_{\rm lift}$ to obtain (5.3).

Now, fix $(\boldsymbol{u},\lambda) \in \mathrm{Ker}(B_h)$ and let $(\boldsymbol{z},\psi)$ be the solution of the auxiliary problem

$$\begin{aligned}
\nabla\times(\mu^{-1}\nabla\times\boldsymbol{z}) - \varepsilon\nabla\psi &= \varepsilon\boldsymbol{u} && \text{in } \Omega,\\
\nabla\cdot(\varepsilon\boldsymbol{z}) &= 0 && \text{in } \Omega,\\
\boldsymbol{n}\times\boldsymbol{z} &= \boldsymbol{0} && \text{on } \Gamma,\\
\psi &= 0 && \text{on } \Gamma.
\end{aligned}$$

In the rest of the proof, we denote by C any constant independent of the mesh size and the coefficients μ and ε, and by C_m any constant that depends on the bounds (2.2) on μ and ε, but is independent of the mesh size.

We have

$$\begin{aligned}
&\|\mu^{-\frac12}\nabla\times\boldsymbol{z}\|_{0,\Omega} + \|\varepsilon^{\frac12}\boldsymbol{z}\|_{0,\Omega} + \|\nabla\times(\mu^{-1}\nabla\times\boldsymbol{z})\|_{0,\Omega}\\
&\qquad + \|\varepsilon^{\frac12}\nabla\psi\|_{0,\Omega} + \|\varepsilon^{\frac12}\psi\|_{0,\Omega} \leq C_m\|\varepsilon^{\frac12}\boldsymbol{u}\|_{0,\Omega}.
\end{aligned} \tag{5.4}$$

Set $\boldsymbol{w} = \mu^{-1}\nabla\times\boldsymbol{z}$; clearly, $\boldsymbol{w} \in H(\mathrm{curl};\Omega)$. Therefore, from [17, Corollary 7.2], there exists $\boldsymbol{w}_0 \in H^1(\Omega)$ such that

$$\nabla\times\boldsymbol{w}_0 = \nabla\times\boldsymbol{w}, \qquad \|\boldsymbol{w}_0\|_{1,\Omega} \leq C\|\boldsymbol{w}\|_{H(\mathrm{curl};\Omega)} \leq C_m\|\varepsilon^{\frac12}\boldsymbol{u}\|_{0,\Omega}. \tag{5.5}$$

Multiplying the first equation of the auxiliary problem by $\boldsymbol{u}$ and integrating by parts over each element, we get

$$\begin{aligned}\|\varepsilon^{\frac{1}{2}}\boldsymbol{u}\|_{0,\Omega}^2 = &\int_\Omega \boldsymbol{w}_0 \cdot \nabla_h \times \boldsymbol{u}\, d\boldsymbol{x} - \int_{\mathcal{F}_h} \boldsymbol{w}_0 \cdot [\![\boldsymbol{u}]\!]_T\, ds \\ &+ \int_\Omega \psi \nabla_h \cdot (\varepsilon \boldsymbol{u})\, d\boldsymbol{x} - \int_{\mathcal{F}_h^{\mathcal{I}}} \{\!\{\psi\}\!\} [\![\varepsilon \boldsymbol{u}]\!]_N\, ds.\end{aligned}$$

Since $(\boldsymbol{u}, \lambda) \in \mathrm{Ker}(B_h)$, we have $B_h(\boldsymbol{u}, \lambda; \psi_h) = 0$ for any $\psi_h \in Q_h$ and obtain, from Remark 2.2 and the fact that $[\![\psi]\!]_N = 0$ on $\mathcal{F}_h$,

$$\begin{aligned}\|\varepsilon^{\frac{1}{2}}\boldsymbol{u}\|_{0,\Omega}^2 = &\int_\Omega \boldsymbol{w}_0 \cdot \nabla_h \times \boldsymbol{u}\, d\boldsymbol{x} - \int_{\mathcal{F}_h} \boldsymbol{w}_0 \cdot [\![\boldsymbol{u}]\!]_T\, ds \\ &+ \int_\Omega (\psi - \psi_h) \nabla_h \cdot (\varepsilon \boldsymbol{u})\, d\boldsymbol{x} - \int_{\mathcal{F}_h^{\mathcal{I}}} \{\!\{\psi - \psi_h\}\!\} [\![\varepsilon \boldsymbol{u}]\!]_N\, ds \\ &- \int_{\mathcal{F}_h} \mathtt{e}\mathtt{h}^{-1} \lambda [\![\psi - \psi_h]\!]_N\, ds.\end{aligned}$$

Using (5.5) and (2.2), we have

$$\left| \int_\Omega \boldsymbol{w}_0 \cdot \nabla_h \times \boldsymbol{u}\, d\boldsymbol{x} \right| \leq C_m \|\boldsymbol{w}_0\|_{1,\Omega} \|\mu^{-\frac{1}{2}} \nabla_h \times \boldsymbol{u}\|_{0,\Omega} \leq C_m \|\varepsilon^{\frac{1}{2}}\boldsymbol{u}\|_{0,\Omega} |\boldsymbol{u}|_{\boldsymbol{V}(h)}.$$

Furthermore, using trace inequalities, (2.2) and (5.5), we obtain

$$\begin{aligned}\left| \int_{\mathcal{F}_h} \boldsymbol{w}_0 \cdot [\![\boldsymbol{u}]\!]_T\, ds \right| &\leq C \Big(\sum_{K \in \mathcal{T}_h} h_K \mu_K \|\boldsymbol{w}_0\|_{0,\partial K}^2 \Big)^{\frac{1}{2}} \|\mathtt{m}^{-\frac{1}{2}} \mathtt{h}^{-\frac{1}{2}} [\![\boldsymbol{u}]\!]_T\|_{0,\mathcal{F}_h} \\ &\leq C_m \|\boldsymbol{w}_0\|_{1,\Omega} \|\mathtt{m}^{-\frac{1}{2}} \mathtt{h}^{-\frac{1}{2}} [\![\boldsymbol{u}]\!]_T\|_{0,\mathcal{F}_h} \leq C_m \|\varepsilon^{\frac{1}{2}}\boldsymbol{u}\|_{0,\Omega} |\boldsymbol{u}|_{\boldsymbol{V}(h)}.\end{aligned}$$

For the other terms, we choose ψ_h as the L^2-projection of ψ on Q_h. Since ε is piecewise constant, we have

$$\int_\Omega (\psi - \psi_h) \nabla_h \cdot (\varepsilon \boldsymbol{u})\, d\boldsymbol{x} = 0.$$

Then, using the Cauchy-Schwarz inequality, the definition of $\mathtt{e}$ and standard approximation properties of the L^2-projection, we obtain

$$\begin{aligned}\left| \int_{\mathcal{F}_h^{\mathcal{I}}} \{\!\{\psi - \psi_h\}\!\} [\![\varepsilon \boldsymbol{u}]\!]_N\, ds \right| &\leq C \big(\sum_{K \in \mathcal{T}_h} \varepsilon_K h_K^{-1} \|\psi - \psi_h\|_{0,\partial K}^2 \big)^{\frac{1}{2}} |\boldsymbol{u}|_{\boldsymbol{V}(h)} \\ &\leq C \big(\sum_{K \in \mathcal{T}_h} \varepsilon_K \|\nabla \psi\|_{0,K}^2 + \varepsilon_K \|\psi\|_{0,K}^2 \big)^{\frac{1}{2}} |\boldsymbol{u}|_{\boldsymbol{V}(h)} \\ &\leq C \big(\|\varepsilon^{\frac{1}{2}} \nabla \psi\|_{0,\Omega}^2 + \|\varepsilon^{\frac{1}{2}} \psi\|_{0,\Omega}^2 \big)^{\frac{1}{2}} |\boldsymbol{u}|_{\boldsymbol{V}(h)} \\ &\leq C_m \|\varepsilon^{\frac{1}{2}}\boldsymbol{u}\|_{0,\Omega} |\boldsymbol{u}|_{\boldsymbol{V}(h)}.\end{aligned}$$

Similarly,

$$\begin{aligned}\left| \int_{\mathcal{F}_h} \mathtt{e}\mathtt{h}^{-1} \lambda [\![\psi - \psi_h]\!]_N\, ds \right| &\leq C \big(\sum_{K \in \mathcal{T}_h} \varepsilon_K h_K^{-1} \|\psi - \psi_h\|_{0,\partial K}^2 \big)^{\frac{1}{2}} \Big(\int_{\mathcal{F}_h} \mathtt{e}\mathtt{h}^{-1} \lambda^2\, ds \Big)^{\frac{1}{2}} \\ &\leq C_m \|\varepsilon^{\frac{1}{2}}\boldsymbol{u}\|_{0,\Omega} \|\lambda\|_{M_h}.\end{aligned}$$

The above computations show that

$$\|\varepsilon^{\frac{1}{2}}\boldsymbol{u}\|_{0,\Omega} \leq C_m\, |(\boldsymbol{u},\lambda)|_{\boldsymbol{W}(h)}.$$

Combining this with (5.3) and the definition of $\|(\boldsymbol{u},\lambda)\|_{\boldsymbol{W}(h)}$ completes the proof. □

5.3. Inf-sup condition. In this section, we prove the inf-sup condition for the form B_h. Our proof is inspired by recent ideas from [7] used in the analysis of stabilized mixed methods.

We will make use of the following technical result: let Q_h^c be the subspace $Q_h \cap H_0^1(\Omega)$ of Q_h, and let $Q_h^\perp$ be the orthogonal complement in Q_h of Q_h^c, with respect to the norm $\|\cdot\|_{Q(h)}$. We observe that

$$\|q\|_{Q_h^\perp} := \|\mathsf{e}^{\frac{1}{2}}\mathbf{h}^{-\frac{1}{2}}[\![q]\!]_N\|_{0,\mathcal{F}_h}$$

is a norm on $Q_h^\perp$. Indeed, if $q \in Q_h^\perp$ and $\|q\|_{Q_h^\perp} = 0$, then $q \in Q_h^\perp \cap Q_h^c = \{0\}$. The norms $\|\cdot\|_{Q_h^\perp}$ and $\|\cdot\|_{Q(h)}$ are equivalent in $Q_h^\perp$.

THEOREM 5.5. *There exist positive constants C_1 and C_2 independent of mesh size and the coefficients μ and ε such that, for any $q \in Q_h^\perp$,*

$$C_1\, \|q\|_{Q(h)} \leq \|q\|_{Q_h^\perp} \leq C_2\, \|q\|_{Q(h)}. \tag{5.6}$$

For the sake of clarity of the presentation, the proof of Theorem 5.5 is postponed to the appendix.

Our main result of this section is the following inf-sup condition.

PROPOSITION 5.6. *We have*

$$\inf_{0\neq q\in Q_h}\ \sup_{\mathbf{0}\,\neq\,(\boldsymbol{v},\nu)\,\in\,\boldsymbol{W}_h} \frac{B_h(\boldsymbol{v},\nu;q)}{\|q\|_{Q(h)}\|(\boldsymbol{v},\nu)\|_{\boldsymbol{W}(h)}} \geq \kappa > 0$$

for a constant κ independent of the mesh size and the coefficients μ and ε.

Proof. Fix $0 \neq q \in Q_h$ and consider its $Q(h)$-orthogonal decomposition as

$$q = q_0 \oplus q_1, \qquad q_0 \in Q_h^c,\ q_1 \in Q_h^\perp. \tag{5.7}$$

By choosing $\boldsymbol{v}_0 = -\nabla q_0 \in \boldsymbol{V}_h \cap H_0(\mathrm{curl}^0;\Omega)$, we have

$$B_h(\boldsymbol{v}_0, 0; q_0) = \|\varepsilon^{\frac{1}{2}}\nabla q_0\|_{0,\Omega}^2 = \|q_0\|_{Q(h)}^2. \tag{5.8}$$

Furthermore, by the definition of e,

$$\begin{aligned}\|(\boldsymbol{v}_0,0)\|_{\boldsymbol{W}(h)}^2 &= \|\mathsf{e}^{-\frac{1}{2}}\mathbf{h}^{\frac{1}{2}}[\![\varepsilon\boldsymbol{v}_0]\!]_N\|_{0,\mathcal{F}_h^{\mathcal{I}}}^2 + \|\varepsilon^{\frac{1}{2}}\boldsymbol{v}_0\|_{0,\Omega}^2\\ &\leq C\sum_{K\in\mathcal{T}_h}\varepsilon_K h_K\|\nabla q_0\|_{0,\partial K}^2 + \|\varepsilon^{\frac{1}{2}}\nabla q_0\|_{0,\Omega}^2\\ &\leq C\sum_{K\in\mathcal{T}_h}\varepsilon_K\|\nabla q_0\|_{0,K}^2 + \|\varepsilon^{\frac{1}{2}}\nabla q_0\|_{0,\Omega}^2\\ &\leq C\|\varepsilon^{\frac{1}{2}}\nabla q_0\|_{0,\Omega}^2 = C\|q_0\|_{Q(h)}^2.\end{aligned} \tag{5.9}$$

Here, we have used the discrete trace inequality

$$\|\nabla\varphi\|_{0,\partial K} \leq Ch_K^{-\frac{1}{2}}\|\nabla\varphi\|_{0,K},$$

valid for polynomials $\varphi \in \mathcal{S}^\ell(K)$, with a constant $C > 0$ that is independent of the local mesh size.

Next, setting $\nu_1 = -[\![q_1]\!]_N$, gives

$$B_h(\mathbf{0}, \nu_1; q_1) = \gamma \int_{\mathcal{F}_h} \mathtt{e}\mathtt{h}^{-1} [\![q_1]\!]_N^2 \, ds \geq \gamma C_1^2 \|q_1\|_{Q(h)}^2, \qquad \|(\mathbf{0}, \nu_1)\|_{\boldsymbol{W}(h)} \leq C_2 \|q_1\|_{Q(h)}, \tag{5.10}$$

where C_1 and C_2 are the constants in the norm-equivalence of Theorem 5.5.

Then, we set

$$(\boldsymbol{v}, \nu) = (\boldsymbol{v}_0, 0) + \delta(\mathbf{0}, \nu_1),$$

with a parameter $\delta > 0$ still at our disposal. Since $B_h(\mathbf{0}, \nu_1; q_0) = 0$, we obtain from (5.8) and (5.10),

$$\begin{aligned} B_h(\boldsymbol{v}, \nu; q) &= B_h(\boldsymbol{v}_0, 0; q_0) + B_h(\boldsymbol{v}_0, 0; q_1) + \delta B_h(\mathbf{0}, \nu_1; q_1) \\ &\geq \|q_0\|_{Q(h)}^2 + \delta\gamma C_1^2 \|q_1\|_{Q(h)}^2 - |B_h(\boldsymbol{v}_0, 0; q_1)|. \end{aligned}$$

Combining the continuity of B_h (see Proposition 5.1) with a weighted Cauchy-Schwarz inequality and (5.9), we obtain for any $\zeta > 0$,

$$|B_h(\boldsymbol{v}_0, 0; q_1)| \leq C\zeta \|\boldsymbol{v}_0\|_{\boldsymbol{V}(h)}^2 + \frac{C}{\zeta} \|q_1\|_{Q(h)}^2 \leq C\zeta \|q_0\|_{Q(h)}^2 + \frac{C}{\zeta} \|q_1\|_{Q(h)}^2.$$

Hence, by suitably choosing δ and ζ, we have

$$B_h(\boldsymbol{v}, \nu; q) \geq \kappa_1 \left[\|q_0\|_{Q(h)}^2 + \|q_1\|_{Q(h)}^2 \right] = \kappa_1 \|q\|_{Q(h)}^2, \tag{5.11}$$

where we also used the $Q(h)$-orthogonality of decomposition (5.7). Finally, from (5.9) and (5.10),

$$\|(\boldsymbol{v}, \nu)\|_{\boldsymbol{W}(h)} \leq \kappa_2 \|q\|_{Q(h)}. \tag{5.12}$$

The constants κ_1 and κ_2 in (5.11) and (5.12) are independent of the mesh size and the coefficients μ and ε. The inf-sup condition follows from (5.11) and (5.12), with $\kappa = \kappa_1/\kappa_2$. $\square$

6. Error estimates. In this section, we prove the error estimates stated in Theorems 3.1, 3.2 and 3.4.

6.1. Abstract error estimates. We start by deriving abstract error bounds. To this end, for the exact solution $(\boldsymbol{u}, p)$ to (2.3)–(2.4), we define the residuals

$$\begin{aligned} R_h^1(\boldsymbol{u}, p; \boldsymbol{v}, \nu) &= A_h(\boldsymbol{u}, 0; \boldsymbol{v}, \nu) + B_h(\boldsymbol{v}, \nu; p) - f_h(\boldsymbol{v}), \\ R_h^2(\boldsymbol{u}; q) &= B_h(\boldsymbol{u}, 0; q) \end{aligned}$$

for all $(\boldsymbol{v}, \nu) \in \boldsymbol{W}_h$ and $q \in Q_h$, and set

$$\mathcal{R}_h^1(\boldsymbol{u}, p) = \sup_{\mathbf{0} \neq (\boldsymbol{v}, \nu) \in \boldsymbol{W}_h} \frac{|R_h^1(\boldsymbol{u}, p; \boldsymbol{v}, \nu)|}{\|(\boldsymbol{v}, \nu)\|_{\boldsymbol{W}(h)}}, \qquad \mathcal{R}_h^2(\boldsymbol{u}) = \sup_{0 \neq q \in Q_h} \frac{|R_h^2(\boldsymbol{u}; q)|}{\|q\|_{Q(h)}}.$$

In the following theorem we present abstract error estimates for our DG method. These error bounds are obtained by straightforwardly extending the standard conforming mixed finite element theory [6] to the setting considered here, and taking into account the residual terms arising from the nonconformity. For the sake of completeness, we present the details of the proof.

THEOREM 6.1. *There exist constants $C > 0$ independent of the mesh size such that*

$$\|(\boldsymbol{u}-\boldsymbol{u}_h,\lambda_h)\|_{\boldsymbol{W}(h)} \leq C\max\{1,b^{-1}\}\Big[\inf_{\boldsymbol{v}\in\boldsymbol{V}_h}\|\boldsymbol{u}-\boldsymbol{v}\|_{\boldsymbol{V}(h)} + \inf_{q\in Q_h}\|p-q\|_{Q(h)} + \mathcal{R}_h^1(\boldsymbol{u},p)+\mathcal{R}_h^2(\boldsymbol{u})\Big], \tag{6.1}$$

and

$$\|p-p_h\|_{Q(h)} \leq C\Big[\inf_{q\in Q_h}\|p-q\|_{Q(h)} + \|(\boldsymbol{u}-\boldsymbol{u}_h,\lambda_h)\|_{\boldsymbol{W}(h)} + \mathcal{R}_h^1(\boldsymbol{u},p)\Big]. \tag{6.2}$$

Here, b, the ellipticity constant from Proposition 5.2, depends on the bounds (2.2) on the coefficients μ and ε, but is independent of the mesh size. The constants C depend on the continuity constants a_1 and a_2 in Proposition 5.1, and on the inf-sup constant κ from Proposition 5.6, but are independent of the mesh size, μ and ε.

Proof. By the triangle inequality and the definition of the norm $\|(\cdot,\cdot)\|_{\boldsymbol{W}(h)}$, we have

$$\|(\boldsymbol{u}-\boldsymbol{u}_h,\lambda_h)\|_{\boldsymbol{W}(h)} \leq \|(\boldsymbol{u}-\boldsymbol{v},\eta)\|_{\boldsymbol{W}(h)} + \|(\boldsymbol{v}-\boldsymbol{u}_h,\eta-\lambda_h)\|_{\boldsymbol{W}(h)}, \tag{6.3}$$

for any $(\boldsymbol{v},\eta)\in\boldsymbol{W}_h$.

We take $(\boldsymbol{v},\eta)\in\mathrm{Ker(B_h)}$. Since $(\boldsymbol{v}-\boldsymbol{u}_h,\eta-\lambda_h)\in\mathrm{Ker(B_h)}$, by using the ellipticity property of Proposition 5.2 and the definition of R_h^1, we have

$$\begin{aligned} b\|(\boldsymbol{v}-\boldsymbol{u}_h,\eta-\lambda_h)\|^2_{\boldsymbol{W}(h)} \leq & A_h(\boldsymbol{v}-\boldsymbol{u}_h,\eta-\lambda_h;\boldsymbol{v}-\boldsymbol{u}_h,\eta-\lambda_h)\\ =& A_h(\boldsymbol{v}-\boldsymbol{u},\eta;\boldsymbol{v}-\boldsymbol{u}_h,\eta-\lambda_h)\\ & - B_h(\boldsymbol{v}-\boldsymbol{u}_h,\eta-\lambda_h;p-q) + R_h^1(\boldsymbol{u},p;\boldsymbol{v}-\boldsymbol{u}_h,\eta-\lambda_h), \end{aligned}$$

for any $q\in Q_h$. From the continuity properties of Proposition 5.1, the definition of the norm $\|(\cdot,\cdot)\|_{\boldsymbol{W}(h)}$ and (6.3), we have

$$\begin{aligned} \|(\boldsymbol{u}-\boldsymbol{u}_h,\lambda_h)\|_{\boldsymbol{W}(h)} \leq & \Big(1+\frac{a_1}{b}\Big)\inf_{(\boldsymbol{v},\eta)\,\in\,\mathrm{Ker(B_h)}}\|(\boldsymbol{u}-\boldsymbol{v},\eta)\|_{\boldsymbol{W}(h)}\\ & + \frac{a_2}{b}\inf_{q\in Q_h}\|p-q\|_{Q(h)} + \frac{1}{b}\mathcal{R}_h^1(\boldsymbol{u},p). \end{aligned} \tag{6.4}$$

Now, we prove that

$$\inf_{(\boldsymbol{v},\eta)\,\in\,\mathrm{Ker(B_h)}}\|(\boldsymbol{u}-\boldsymbol{v},\eta)\|_{\boldsymbol{W}(h)} \leq \Big(1+\frac{a_2}{\kappa}\Big)\inf_{(\boldsymbol{v},\eta)\,\in\,\boldsymbol{W}_h}\|(\boldsymbol{u}-\boldsymbol{v},\eta)\|_{\boldsymbol{W}(h)} + \frac{1}{\kappa}\mathcal{R}_h^2(\boldsymbol{u}). \tag{6.5}$$

To this end, let $(\boldsymbol{v},\eta)$ be any element of $\boldsymbol{W}_h$, and consider the following problem: find $(\boldsymbol{w},\nu)\in\boldsymbol{W}_h$ such that

$$B_h(\boldsymbol{w},\nu;q) = B_h(\boldsymbol{u}-\boldsymbol{v},-\eta;q) - R_h^2(\boldsymbol{u},q) \qquad \forall q\in Q_h. \tag{6.6}$$

Problem (6.6) admits solutions in $\boldsymbol{W}_h$ that are unique up to the kernel of B_h. The discrete inf-sup condition of Proposition 5.6 guarantees the existence of a solution

$(\boldsymbol{w}, \nu)$ satisfying

$$\begin{aligned} \|(\boldsymbol{w}, \nu)\|_{\boldsymbol{W}(h)} &\leq \frac{1}{\kappa}\Big[\sup_{q \in Q_h} \frac{|B_h(\boldsymbol{u}-\boldsymbol{v}, -\eta; q)|}{\|q\|_{Q(h)}} + \sup_{q \in Q_h} \frac{|R_h^2(\boldsymbol{u}, q)|}{\|q\|_{Q(h)}}\Big] \\ &\leq \frac{a_2}{\kappa}\|(\boldsymbol{u}-\boldsymbol{v}, \eta)\|_{\boldsymbol{W}(h)} + \frac{1}{\kappa}\mathcal{R}_h^2(\boldsymbol{u}), \end{aligned} \tag{6.7}$$

where we have used the continuity of B_h, the definition of the norm $\|(\cdot,\cdot)\|_{\boldsymbol{W}(h)}$, and the definition of $\mathcal{R}_h^2$. From (6.6), $B_h(\boldsymbol{w}+\boldsymbol{v}, \nu+\eta; q) = 0$, for any $q \in Q_h$, so that $(\boldsymbol{w}+\boldsymbol{v}, \nu+\eta) \in \operatorname{Ker}(B_h)$. Therefore, since

$$\|(\boldsymbol{u}-(\boldsymbol{v}+\boldsymbol{w}), \eta+\nu)\|_{\boldsymbol{W}(h)} \leq \|(\boldsymbol{u}-\boldsymbol{v}, \eta)\|_{\boldsymbol{W}(h)} + \|(\boldsymbol{w}, \nu)\|_{\boldsymbol{W}(h)},$$

for any $(\boldsymbol{v}, \eta) \in \boldsymbol{W}_h$, taking into account (6.7), we obtain (6.5). This, together with (6.4), yields

$$\begin{aligned} \|(\boldsymbol{u}-\boldsymbol{u}_h, \lambda_h)\|_{\boldsymbol{W}(h)} \leq C\max\{1, b^{-1}\}\Big[&\inf_{(\boldsymbol{v},\eta) \in \boldsymbol{W}_h} \|(\boldsymbol{u}-\boldsymbol{v}, \eta)\|_{\boldsymbol{W}(h)} \\ &+ \inf_{q \in Q_h} \|p-q\|_{Q(h)} + \mathcal{R}_h^1(\boldsymbol{u}, p) + \mathcal{R}_h^2(\boldsymbol{u})\Big], \end{aligned}$$

where the constant C depends on a_1, a_2, and κ. Choosing $\eta = 0$, gives (6.1).

Let us now turn to (6.2). Again by the triangle inequality, we have

$$\|p-p_h\|_{Q(h)} \leq \|p-q\|_{Q(h)} + \|q-p_h\|_{Q(h)}, \tag{6.8}$$

for any $q_h \in Q_h$. Since

$$A_h(\boldsymbol{u}-\boldsymbol{u}_h, -\lambda_h; \boldsymbol{v}, \eta) + B_h(\boldsymbol{v}, \eta; p-q) + B_h(\boldsymbol{v}, \eta; q-p_h) = R_h^1(\boldsymbol{u}, p; \boldsymbol{v}, \eta),$$

for any $(\boldsymbol{v}, \eta) \in \boldsymbol{W}_h$, the discrete inf-sup condition of Proposition 5.6 gives

$$\begin{aligned} \|q-p_h\|_{Q(h)} &\leq \frac{1}{\kappa} \sup_{(\mathbf{0},0) \neq (\boldsymbol{v},\eta) \in \boldsymbol{W}_h} \frac{B_h(\boldsymbol{v}, \eta; q-p_h)}{\|(\boldsymbol{v}, \eta)\|_{\boldsymbol{W}(h)}} \\ &= \frac{1}{\kappa} \sup_{(\mathbf{0},0) \neq (\boldsymbol{v},\eta) \in \boldsymbol{W}_h} \frac{-A_h(\boldsymbol{u}-\boldsymbol{u}_h, -\lambda_h; \boldsymbol{v}, \eta) - B_h(\boldsymbol{v}, \eta; p-q) + R_h^1(\boldsymbol{u}, p; \boldsymbol{v}, \eta)}{\|(\boldsymbol{v}, \eta)\|_{\boldsymbol{W}(h)}} \\ &\leq \frac{a_1}{\kappa}\|(\boldsymbol{u}-\boldsymbol{u}_h, \lambda_h)\|_{\boldsymbol{W}(h)} + \frac{a_2}{\kappa}\|p-q\|_{Q(h)} + \frac{1}{\kappa}\mathcal{R}_h^1(\boldsymbol{u}, p). \end{aligned}$$

This, together with (6.8), gives (6.2). □

6.2. Proof of Theorem 3.1 and Theorem 3.2. We are now ready to prove our main results, by making explicit the abstract error estimates of Theorem 6.1.

First, we show the following estimates of the residuals. We note that the residuals are optimally convergent on possibly nonconforming meshes under minimal smoothness assumptions as in Theorem 3.2, thereby covering both the cases of Theorem 3.1 and Theorem 3.2.

PROPOSITION 6.2. *Let $\mathcal{T}_h$ be a possibly nonconforming mesh satisfying the restrictions (i) and (ii) in Section 3.2. Assume the exact solution $(\boldsymbol{u}, p)$ of (2.1) satisfies $\varepsilon\boldsymbol{u} \in H^s(\mathcal{T}_h)^3$ and $\mu^{-1}\nabla \times \boldsymbol{u} \in H^s(\mathcal{T}_h)^3$, for $s > \frac{1}{2}$. Then we have*

$$\mathcal{R}_h^1(\boldsymbol{u}, p) + \mathcal{R}_h^2(\boldsymbol{u}) \leq Ch^{\min\{s, \ell+1\}}\big[\|\varepsilon\boldsymbol{u}\|_{s,\mathcal{T}_h} + \|\mu^{-1}\nabla \times \boldsymbol{u}\|_{s,\mathcal{T}_h}\big],$$

with a constant $C > 0$ independent of the mesh size.

Proof. First, for $\boldsymbol{v} \in \boldsymbol{V}_h$, $\eta \in M_h$, we have

$$|R_h^1(\boldsymbol{u}, p; \boldsymbol{v}, \eta)| = |\int_{\mathcal{F}_h} \{\!\!\{\mu^{-1}\nabla \times \boldsymbol{u} - \boldsymbol{\Pi}_{\boldsymbol{V}_h}(\mu^{-1}\nabla \times \boldsymbol{u})\}\!\!\} \cdot [\![\boldsymbol{v}]\!]_T \, ds|,$$

with $\boldsymbol{\Pi}_{\boldsymbol{V}_h}$ denoting the L^2-projection onto $\boldsymbol{V}_h$. This can be easily seen by integration by parts, by using properties of the L^2-projection and by taking into account the first equation in (2.1). From the Cauchy-Schwarz inequality and standard approximation properties, we obtain

$$\begin{aligned} |R_h^1(\boldsymbol{u}, \lambda, p; \boldsymbol{v}, \eta)| &\leq C\Big(\sum_{K \in \mathcal{T}_h} h_K \|\mu^{-1}\nabla \times \boldsymbol{u} - \boldsymbol{\Pi}_{\boldsymbol{V}_h}(\mu^{-1}\nabla \times \boldsymbol{u})\|_{0,\partial K}^2\Big)^{\frac{1}{2}} \|(\boldsymbol{v}, \eta)\|_{\boldsymbol{W}(h)} \\ &\leq C h^{\min\{s, \ell+1\}} \|\mu^{-1}\nabla \times \boldsymbol{u}\|_{s,\mathcal{T}_h} \|(\boldsymbol{v}, \eta)\|_{\boldsymbol{W}(h)}. \end{aligned}$$

Furthermore, for $q \in Q_h$,

$$|R_h^2(\boldsymbol{u}; q)| = \left| \int_{\mathcal{F}_h} \{\!\!\{\varepsilon \boldsymbol{u} - \boldsymbol{\Pi}_{\boldsymbol{V}_h}(\varepsilon \boldsymbol{u})\}\!\!\} \cdot [\![q]\!]_N \, ds \right|.$$

Hence,

$$\begin{aligned} |R_h^2(\boldsymbol{u}; q)| &\leq C\Big(\sum_{K \in \mathcal{T}_h} h_K \|\varepsilon \boldsymbol{u} - \boldsymbol{\Pi}_{\boldsymbol{V}_h}(\varepsilon \boldsymbol{u})\|_{0,\partial K}^2\Big)^{\frac{1}{2}} \|q\|_{Q(h)} \\ &\leq C h^{\min\{s, \ell+1\}} \|\varepsilon \boldsymbol{u}\|_{s,\mathcal{T}_h} \|q\|_{Q(h)}. \end{aligned}$$

This completes the proof (the constant C in these estimates actually depends on the bound (2.2) on the coefficients μ and ε). $\square$

Next, we prove the result of Theorems 3.1 and 3.2.

Proof of Theorem 3.1: Let $(\boldsymbol{u}_h, p_h, \lambda_h)$ be the solution of the auxiliary mixed system in (4.3)–(4.4). We apply Theorem 6.1 and bound all the terms on the right–hand side of (6.1) and (6.2). To this end, we set $\boldsymbol{v} = \boldsymbol{\Pi}_{\boldsymbol{V}_h}\boldsymbol{u}$ in (6.1)–(6.2), with $\boldsymbol{\Pi}_{\boldsymbol{V}_h}$ denoting the L^2–projection onto $\boldsymbol{V}_h$. The additional smoothness assumption on $\boldsymbol{u}$ made in this case is required for the estimate of the term containing the tangential jumps. Standard approximation properties of the L^2–projection, together with the bounded variation of the local mesh size (3.2), give

$$\|\boldsymbol{u} - \boldsymbol{\Pi}_{\boldsymbol{V}_h}\boldsymbol{u}\|_{\boldsymbol{V}(h)} \leq C\, h^{\min\{s,\ell\}} \|\boldsymbol{u}\|_{s+1,\mathcal{T}_h}.$$

Similarly, we choose $q = \Pi_{Q_h} p$, the L^2–projection of p on Q_h and obtain

$$\|p - \Pi_{Q_h} p\|_{Q(h)} \leq C\, h^{\min\{s,\ell\}} \|p\|_{s+1,\mathcal{T}_h}.$$

The constants C in the previous estimates also depend on the bounds (2.2) on the coefficients μ and ε. Inserting these estimates, together with the residual estimates of Proposition 6.2, in Theorem 6.1 gives the result. $\square$

Proof of Theorem 3.2: Let $(\boldsymbol{u}_h, p_h, \lambda_h)$ be the solution of the auxiliary mixed system in (4.3)–(4.4). As in the proof of Theorem 3.1, we apply Theorem 6.1. On conforming meshes, we can choose $\boldsymbol{v} = \boldsymbol{\Pi}_{\mathrm{curl}}\boldsymbol{u} \in H(\mathrm{curl}; \Omega)$ in (6.1)–(6.2) as the standard conforming Nédéléc interpolant of $\boldsymbol{u}$ of the second type; see [23]. Thereby, we have $[\![\boldsymbol{v}]\!]_T = \mathbf{0}$ on $\mathcal{F}_h^{\mathcal{I}}$ and from the approximation results proved in [2] for tetrahedra, but also valid for parallelepipeds, we get

$$\|\boldsymbol{u} - \boldsymbol{\Pi}_{\mathrm{curl}}\boldsymbol{u}\|_{0,K} + \|\nabla \times (\boldsymbol{u} - \boldsymbol{\Pi}_{\mathrm{curl}}\boldsymbol{u})\|_{0,K} \leq C\, h_K^{\min\{s,\ell\}} \big[\|\boldsymbol{u}\|_{s,K} + \|\nabla \times \boldsymbol{u}\|_{s,K}\big].$$

Hence,

$$\begin{aligned}\|\varepsilon^{\frac{1}{2}}(\boldsymbol{u} - \boldsymbol{\Pi}_{\mathrm{curl}}\boldsymbol{u})\|_{0,\Omega} + \|\mu^{-\frac{1}{2}}\nabla \times (\boldsymbol{u} - \boldsymbol{\Pi}_{\mathrm{curl}}\boldsymbol{u})\|_{0,\Omega}& \\ \leq C\, h^{\min\{s,\ell\}} \big[\|\varepsilon\boldsymbol{u}\|_{s,\mathcal{T}_h} + \|\mu^{-1}\nabla \times \boldsymbol{u}\|_{s,\mathcal{T}_h}\big],&\end{aligned} \tag{6.9}$$

with C also depending on the bounds (2.2) on the coefficients μ and ε. On a boundary face $f \subset \mathcal{F}_h^{\mathcal{D}}$, the tangential field $\boldsymbol{n}\times\boldsymbol{\Pi}_{\mathrm{curl}}\boldsymbol{u}$ coincides with $\boldsymbol{\Pi}_{\mathrm{div}}(\boldsymbol{n}\times\boldsymbol{u})$, where $\boldsymbol{\Pi}_{\mathrm{div}}$ is the two-dimensional $H(\mathrm{div})$-conforming Nédélec interpolation operator of the second type. In particular, $\boldsymbol{\Pi}_{\mathrm{div}}$ reproduces polynomial tangential fields of degree ℓ on f; see [23] for details. From a standard scaling arguments, we obtain

$$\|\boldsymbol{n} \times (\boldsymbol{u} - \boldsymbol{\Pi}_{\mathrm{curl}}\boldsymbol{u})\|_{0,f} \leq C\, \mathtt{h}_{|f}^{\min\{s,\ell\}+\frac{1}{2}} \|\boldsymbol{g}\|_{s+\frac{1}{2},f}.$$

Therefore, summing over all faces yields

$$\|\mathtt{m}^{-\frac{1}{2}}\mathtt{h}^{-\frac{1}{2}}(\boldsymbol{n} \times \boldsymbol{u} - \boldsymbol{\Pi}_{\mathrm{curl}}(\boldsymbol{n} \times \boldsymbol{u}))\|_{0,\mathcal{F}_h^{\mathcal{D}}} \leq C\, h^{\min\{s,\ell\}} \|\boldsymbol{g}\|_{s+\frac{1}{2},\mathcal{F}_h^{\mathcal{D}}}. \tag{6.10}$$

Moreover, since $\boldsymbol{u}$ also belongs to $H(\mathrm{div}_\varepsilon^0;\Omega)$, we have for an interior face f, shared by K_f and K_f',

$$\|\mathtt{e}^{-\frac{1}{2}}\mathtt{h}^{\frac{1}{2}}[\![\varepsilon(\boldsymbol{u} - \boldsymbol{\Pi}_{\mathrm{curl}}\boldsymbol{u})]\!]_N\|_{0,f} \leq C\, h^{\min\{s,\ell\}} \big[\|\boldsymbol{u}\|_{s,K_f\cup K_f'} + \|\nabla \times \boldsymbol{u}\|_{s,K_f\cup K_f'}\big].$$

This bound follows from [25, Lemma 23]. Hence,

$$\|\mathtt{e}^{-\frac{1}{2}}\mathtt{h}^{\frac{1}{2}}[\![\varepsilon(\boldsymbol{u} - \boldsymbol{\Pi}_{\mathrm{curl}}\boldsymbol{u})]\!]_N\|_{0,\mathcal{F}_h^{\mathcal{I}}} \leq C\, \big[\|\varepsilon\boldsymbol{u}\|_{s,\mathcal{T}_h} + \|\mu^{-1}\nabla \times \boldsymbol{u}\|_{s,\mathcal{T}_h}\big]. \tag{6.11}$$

Moreover, choosing $q = \Pi_{H^1}p$ in (6.1)–(6.2) where Π_{H^1} is a standard H^1-projector, we have $[\![q]\!]_N = 0$ on $\mathcal{F}_h$ and

$$\|p - \Pi_{H^1}p\|_{Q(h)} \leq C\, h^{\min\{s,\ell\}} \|p\|_{s+1,\mathcal{T}_h}. \tag{6.12}$$

Combining (6.9)–(6.12) with the residual estimates in Proposition 6.2 yields

$$\begin{aligned}\inf_{\boldsymbol{v}\,\in\,\boldsymbol{V}_h} \|\boldsymbol{u} - \boldsymbol{v}\|_{\boldsymbol{V}(h)} + \inf_{q\in Q_h} \|p - q\|_{Q(h)} + \mathcal{R}_h^1(\boldsymbol{u},p) + \mathcal{R}_h^2(\boldsymbol{u})& \\ \leq C\, h^{\min\{s,\ell\}} \big[\|\varepsilon\boldsymbol{u}\|_{s,\mathcal{T}_h} + \|\mu^{-1}\nabla \times \boldsymbol{u}\|_{s,\mathcal{T}_h} + \|p\|_{s+1,\mathcal{T}_h} + \|\boldsymbol{g}\|_{s+\frac{1}{2},\mathcal{F}_h^{\mathcal{D}}}\big],&\end{aligned}$$

with C also depending on the bounds (2.2) on the coefficients μ and ε. Again, combining these estimates with the residual estimates of Proposition 6.2 gives the result. ∎

6.3. Proof of Theorem 3.4. To prove Theorem 3.4, we first recall that

$$B_h(\boldsymbol{u}_h, \lambda_h; q) = 0 \qquad \forall q \in Q_h.$$

Note that $\lambda_h = [\![p]\!]_N$, cf. Proposition 4.1; thereby, for an element $K \in \mathcal{T}_h$, we have

$$-\int_K \varepsilon\boldsymbol{u}_h \cdot \nabla q\, d\boldsymbol{x} + \int_{\partial K} \{\!\{\varepsilon\boldsymbol{u}_h\}\!\} \cdot (q\boldsymbol{n}_K)\, ds - \gamma\frac{\mathtt{e}}{\mathtt{h}} \int_{\partial K} [\![p_h]\!] \cdot (q\boldsymbol{n}_K)\, ds = 0 \tag{6.13}$$

for all $q \in \mathcal{S}^\ell(K)$. Employing integration by parts and the identity (6.13), we get, after some elementary manipulations, the following

$$\begin{aligned} h_K \int_K \nabla \cdot (\varepsilon \boldsymbol{u}_h) q \, d\boldsymbol{x} &= -h_K \int_K \varepsilon \boldsymbol{u}_h \cdot \nabla q \, d\boldsymbol{x} + h_K \int_{\partial K} \varepsilon \boldsymbol{u}_h \cdot (q \boldsymbol{n}_K) \, ds \\ &= h_K \int_{\partial K^0} [\![\varepsilon \boldsymbol{u}_h]\!]_N q \, ds + h_K \gamma \frac{\mathtt{e}}{\mathtt{h}} \int_{\partial K} [\![p_h]\!] \cdot (q \boldsymbol{n}_K) \, ds, \end{aligned}$$

for $q \in \mathcal{S}^\ell(K)$, where $\partial K^0 = \partial K \cap \mathcal{F}_h^{\mathcal{I}}$. The Cauchy-Schwarz inequality gives

$$|h_K \int_K \nabla \cdot (\varepsilon \boldsymbol{u}_h) q \, d\boldsymbol{x}| \leq C h_K^{-\frac{1}{2}} \|q\|_{0,\partial K} \Big(\int_{\partial K^0} \mathtt{h} [\![\varepsilon \boldsymbol{u}_h]\!]_N^2 \, ds + \int_{\partial K} \frac{\mathtt{e}}{\mathtt{h}} [\![p_h]\!]_N^2 \, ds \Big)^{\frac{1}{2}},$$

with a constant $C > 0$ independent of the mesh size. Here, we used (3.2) and the shape-regularity of the mesh. Employing the discrete trace inequality

$$\|q\|_{0,\partial K} \leq C h_K^{-1} \|q\|_{0,K}^2 \qquad \forall q \in \mathcal{S}^\ell(K),$$

and the characterization

$$h_K \|\nabla \cdot (\varepsilon \boldsymbol{u}_h)\|_{0,K} = \sup_{q \in \mathcal{S}^\ell(K)} \frac{h_K \int_K \nabla \cdot (\varepsilon \boldsymbol{u}_h) q \, d\boldsymbol{x}}{\|q\|_{0,K}},$$

we obtain

$$h_K^2 \|\nabla \cdot (\varepsilon \boldsymbol{u}_h)\|_{0,K}^2 \leq C \Big(\int_{\partial K^0} \mathtt{h} [\![\varepsilon \boldsymbol{u}_h]\!]_N^2 \, ds + \int_{\partial K} \frac{\mathtt{e}}{\mathtt{h}} [\![p_h]\!]_N^2 \, ds \Big).$$

Summing over all elements and taking into account that the exact solution satisfies $[\![\varepsilon \boldsymbol{u}]\!]_N = 0$ on $\mathcal{F}_h^{\mathcal{I}}$ and $[\![p]\!]_N = \boldsymbol{0}$ on $\mathcal{F}_h$ completes the proof of Theorem 3.4. □

7. Numerical experiments. In this section, we present a series of numerical experiments to illustrate the a priori error estimates derived for the mixed DG method introduced in Section 2. Here, we restrict ourselves to two-dimensional model problems with constant coefficients $\mu \equiv \varepsilon \equiv 1$. In this case, by identifying two-dimensional vector fields $\boldsymbol{u}(x,y) = (u_1(x,y), u_2(x,y))$ in $\mathbb{R}^2$ with their three-dimensional extensions $\boldsymbol{u}(x,y,z) = (u_1(x,y,0), u_2(x,y,0), 0)$ in $\mathbb{R}^3$, we deduce that

$$\nabla \times (\nabla \times \boldsymbol{u}) = \left(\frac{\partial}{\partial y} \left(\frac{\partial u_2}{\partial x} - \frac{\partial u_1}{\partial y} \right), -\frac{\partial}{\partial x} \left(\frac{\partial u_2}{\partial x} - \frac{\partial u_1}{\partial y} \right) \right).$$

On the boundary, we have $\boldsymbol{n} \times \boldsymbol{u} = \boldsymbol{u} \cdot \boldsymbol{t}$, where $\boldsymbol{t}$ is the counterclockwise oriented tangential unit vector, i.e., if $\boldsymbol{n} = (n_1, n_2)$, then $(t_1, t_2) = (-n_2, n_1)$. Hence, the Dirichlet boundary datum given in (2.1) is a scalar function g. Similarly, the tangential jumps are scalar quantities defined as $[\![\boldsymbol{u}]\!]_T = \boldsymbol{u}^+ \cdot \boldsymbol{t}^+ + \boldsymbol{u}^- \cdot \boldsymbol{t}^-$.

Finally, we note that throughout this section we select the constants appearing in the stabilization parameters defined in (3.1) as follows:

$$\alpha = 10\,\ell^2, \quad \beta = 1 \;\text{ and }\; \gamma = 1.$$

We remark that the dependence of α on the polynomial degree ℓ has been formally chosen in order to guarantee the stability of the underlying DG discretization independently of ℓ, cf. [19], for example.

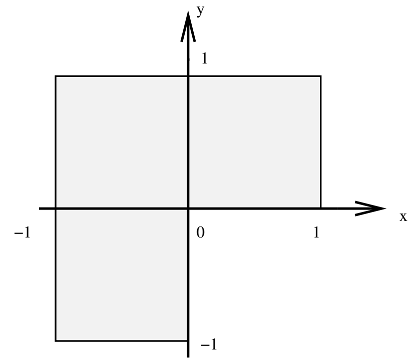

FIG. 7.1. *L-shaped domain* Ω.

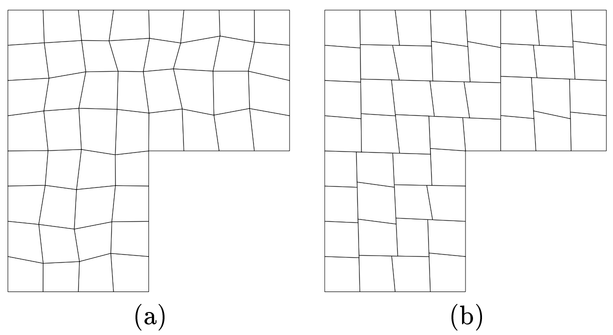

FIG. 7.2. *Example 1. (a) Quadrilateral mesh (i); (b) Quadrilateral mesh (ii).*

7.1. Example 1. Here, we let Ω be the L-shaped domain shown in Figure 7.1; further, we choose $\boldsymbol{j}$ and g so that the analytical solution to the two-dimensional analogue of (2.1) with $\mu \equiv \varepsilon \equiv 1$ is given by

$$\begin{pmatrix} u_1 \\ u_2 \\ p \end{pmatrix} = \begin{pmatrix} -\exp(x)(y\cos(y) + \sin(y)) \\ \exp(x)y\sin(y) \\ \sin(\pi(x-1)/2)\sin(\pi(y-1)/2) \end{pmatrix}; \tag{7.1}$$

this is a variant of the model problem considered in [19]. We investigate the asymptotic behavior of the errors of the mixed DG method (2.5)–(2.6) on a sequence of successively finer square and quadrilateral meshes for different values of the polynomial degree ℓ. In each case we consider two types of quadrilateral mesh which are constructed from a uniform square mesh by (i) randomly perturbing each of the interior nodes by up to 10% of the local mesh size, cf. Figure 7.2(a); (ii) randomly *splitting* each of the interior nodes by a displacement of up to 10% of the local mesh size, cf. Figure 7.2(b). The latter meshes are constructed so that all the nodes in the interior of Ω are irregular (i.e., hanging), cf. [20]. We note that the meshes in cases (i) and (ii) are not rigorously covered by our theory since they are non-affine and need to be bilinearly mapped onto the reference square.

In Figure 7.3 we first present a comparison of the DG–norm $\|\cdot\|_{\boldsymbol{V}(h)}$ of the error in the approximation to $\mathbf{u}$ with the mesh function h for $1 \leq \ell \leq 4$. For consistency, $\|\boldsymbol{u} - \boldsymbol{u}_h\|_{\boldsymbol{V}(h)}$ is plotted against h_u for each mesh type, where h_u denotes the mesh size of the uniform square mesh; this ensures that a fair comparison between the

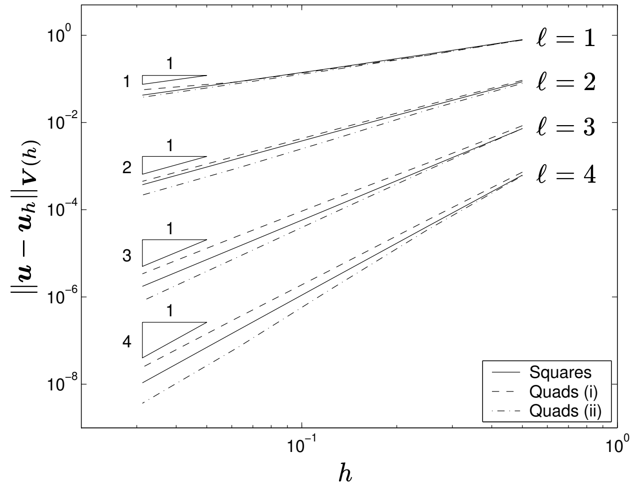

FIG. 7.3. *Example 1. Convergence of* $\|\boldsymbol{u} - \boldsymbol{u}_h\|_{\boldsymbol{V}(h)}$ *with* h*–refinement.*

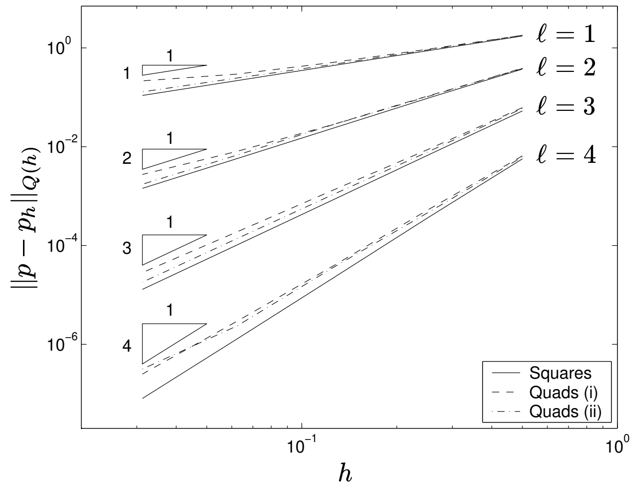

FIG. 7.4. *Example 1. Convergence of* $\|p - p_h\|_{Q(h)}$ *with* h*-refinement.*

error per degree of freedom for each mesh type can be made. Here, we observe that $\|\boldsymbol{u} - \boldsymbol{u}_h\|_{\boldsymbol{V}(h)}$ converges to zero, for each fixed ℓ, at the rate $\mathcal{O}(h^\ell)$ as the mesh is refined, thereby confirming Theorem 3.1. In particular, we observe that while the error on the square mesh is smaller than on the randomly generated quadrilateral mesh (i), as we would expect, the error is consistently smaller when the irregular quadrilateral mesh is employed. As in [20], we attribute this improvement in $\|\boldsymbol{u} - \boldsymbol{u}_h\|_{\boldsymbol{V}(h)}$ to the increase in inter-element communication on the meshes (ii); when no hanging nodes are present in the mesh, elements may only communicate with their four immediate neighbors. On the other hand, on irregular meshes elements may now communicate with all of their neighbors which share a common node, cf. [20].

Secondly, in Figure 7.4 we plot the DG–norm $\|\cdot\|_{Q(h)}$ of the error in approximating p by p_h as the mesh size tends to zero. As for the approximation to $\boldsymbol{u}$, we again observe that $\|p - p_h\|_{Q(h)}$ converges to zero, for each fixed ℓ, at the rate $\mathcal{O}(h^\ell)$ as

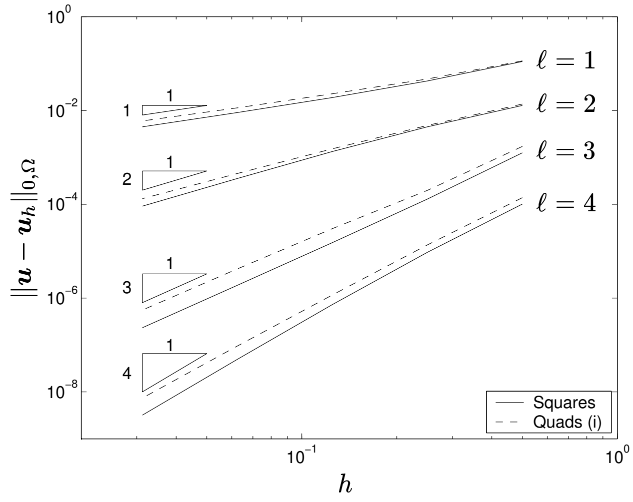

FIG. 7.5. *Example 1. Convergence of* $\|\boldsymbol{u}-\boldsymbol{u}_h\|_{0,\Omega}$ *with* h*-refinement.*

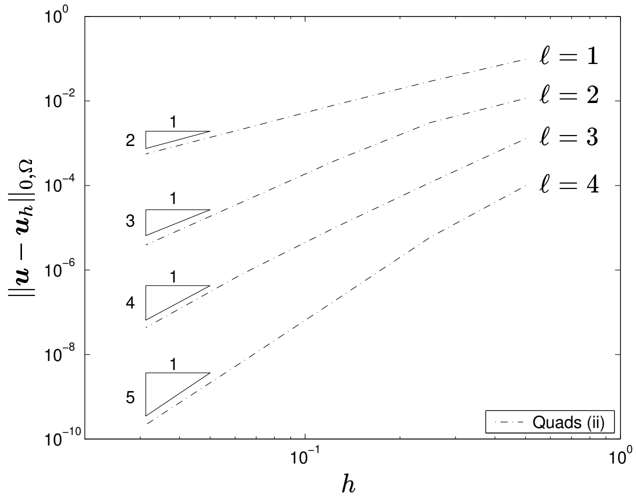

FIG. 7.6. *Example 1. Convergence of* $\|\boldsymbol{u}-\boldsymbol{u}_h\|_{0,\Omega}$ *with* h*-refinement.*

the mesh is refined, cf. Theorem 3.1. However, in contrast to the approximation to $\boldsymbol{u}$, both the conforming and nonconforming quadrilateral meshes lead to a slight degradation in the size of the error in the approximation to p for each mesh and each polynomial degree employed; though, in almost all cases the error in the numerical solution computed on the meshes (ii) was observed to be slightly smaller than the corresponding quantity computed on the meshes (i). Thereby, the increase in inter-element communication arising when the nonconforming quadrilateral meshes (ii) are employed no longer leads to the improvement in the size of the approximation error observed above for $\boldsymbol{u}$ as well as in [20].

The increase in the quality of the numerical approximation $\boldsymbol{u}_h$ to $\boldsymbol{u}$ when the nonconforming meshes (ii) are employed becomes even more apparent when the error $\boldsymbol{u}-\boldsymbol{u}_h$ is measured in terms of the $L^2(\Omega)$–norm. To this end, in Figure 7.5, we first plot

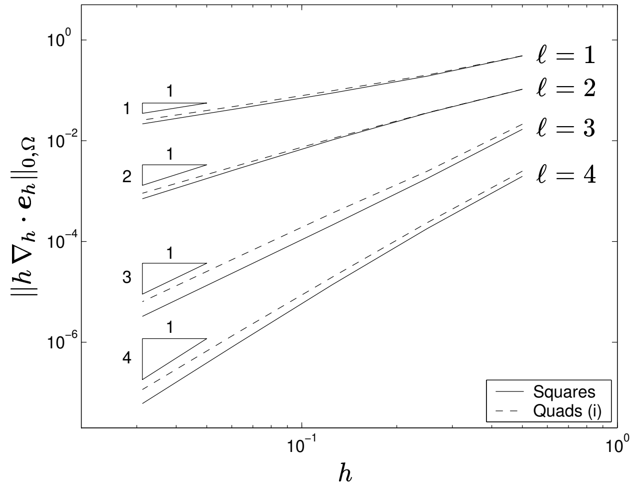

FIG. 7.7. *Example 1. Convergence of* $\|h\,\nabla_h \cdot \boldsymbol{e}_h\|_{0,\Omega}$ *with h-refinement.*

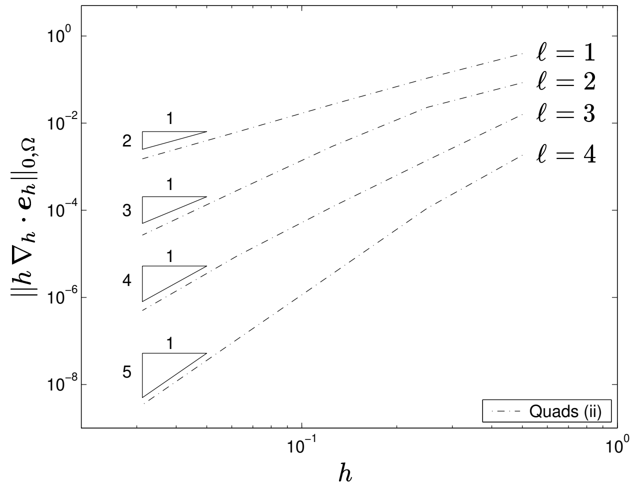

FIG. 7.8. *Example 1. Convergence of* $\|h\,\nabla_h \cdot \boldsymbol{e}_h\|_{0,\Omega}$ *with h-refinement.*

$\|\boldsymbol{u} - \boldsymbol{u}_h\|_{0,\Omega}$ against h for $1 \leq \ell \leq 4$ using the uniform square and randomly generated quadrilateral meshes (i). As predicted by Theorem 3.1, we observe that $\|\boldsymbol{u} - \boldsymbol{u}_h\|_{0,\Omega}$ converges to zero, for each fixed ℓ, at the rate $\mathcal{O}(h^{\ell})$ as the mesh is refined. While this rate of convergence is one order less than we would expect when using discontinuous piecewise polynomials of degree at most ℓ in each coordinate direction, the numerical results clearly verify the sharpness of the a priori error analysis. However, in contrast, when the nonconforming quadrilateral meshes (ii) are employed, the order of convergence increases by a full power of h; thereby, in this case $\|\boldsymbol{u} - \boldsymbol{u}_h\|_{0,\Omega}$ now converges to zero, for each fixed ℓ, at the rate $\mathcal{O}(h^{\ell+1})$ as h tends to zero, cf. Figure 7.6. Analogous behavior is also observed when the $L^2(\Omega)$–norm of the error in the approximation to the divergence of $\boldsymbol{u}$ is computed. Indeed, from Figure 7.7, we observe that $\|h\,\nabla_h \cdot \boldsymbol{e}_h\|_{0,\Omega} := (\sum_{K \in \mathcal{T}_h} h_K^2 \|\nabla \cdot (\boldsymbol{u} - \boldsymbol{u}_h)\|_{0,K}^2)^{\frac{1}{2}}$ converges to zero at the rate $\mathcal{O}(h^{\ell})$ as h tends to zero, when the uniform and randomly generated quadrilateral

	$\ell = 1$		$\ell = 2$		$\ell = 3$	
Elements	$\Vert \boldsymbol{u} - \boldsymbol{u}_h \Vert_{\boldsymbol{V}(h)}$	k	$\Vert \boldsymbol{u} - \boldsymbol{u}_h \Vert_{\boldsymbol{V}(h)}$	k	$\Vert \boldsymbol{u} - \boldsymbol{u}_h \Vert_{\boldsymbol{V}(h)}$	k
12	5.987e-1	-	5.350e-1	-	4.853e-1	-
48	4.300e-1	0.48	3.427e-1	0.64	3.076e-1	0.66
192	2.815e-1	0.61	2.144e-1	0.68	1.929e-1	0.67
768	1.816e-1	0.63	1.344e-1	0.67	1.211e-1	0.67
3072	1.170e-1	0.63	8.452e-2	0.67	7.622e-2	0.67

TABLE 7.1

Example 2. Convergence of $\Vert \boldsymbol{u} - \boldsymbol{u}_h \Vert_{\boldsymbol{V}(h)}$ *on uniform square meshes with h–refinement.*

	$\ell = 1$		$\ell = 2$		$\ell = 3$	
Elements	$\Vert p - p_h \Vert_{Q(h)}$	k	$\Vert p - p_h \Vert_{Q(h)}$	k	$\Vert p - p_h \Vert_{Q(h)}$	k
12	8.742e-1	-	1.341	-	1.598	-
48	8.147e-1	0.10	1.039	0.37	1.178	0.44
192	6.235e-1	0.39	7.159e-1	0.54	7.948e-1	0.57
768	4.253e-1	0.55	4.678e-1	0.61	5.154e-1	0.63
3072	2.763e-1	0.62	2.990e-1	0.65	3.285e-1	0.65

TABLE 7.2

Example 2. Convergence of $\Vert p - p_h \Vert_{Q(h)}$ *on uniform square meshes with h–refinement.*

meshes (i) are employed, thereby confirming Theorem 3.4 and Remark 3.5. On the other hand, when the nonconforming quadrilateral meshes (ii) are employed, this rate of convergence increases to $\mathcal{O}(h^{\ell+1})$ as h tends to zero, cf. Figure 7.8.

As a final remark, we note that on all the meshes employed, the $L^2(\Omega)$–norm of the error in the approximation to p converges to zero, for each fixed ℓ, at the (optimal) rate $\mathcal{O}(h^{\ell+1})$ as the mesh is refined. As for the DG–norm of $p - p_h$, both the conforming and nonconforming quadrilateral meshes lead to a slight degradation in the size of $\Vert p - p_h \Vert_{0,\Omega}$ for each mesh and each polynomial degree employed, though the error in the numerical solution computed on the meshes (ii) was observed to be slightly smaller than the corresponding quantity computed on the meshes (i); for brevity, these results have been omitted.

7.2. Example 2. In this second example, we investigate the performance of the mixed DG method (2.5)–(2.6) for a problem with a corner singularity in $\mathbf{u}$. To this end, we again let Ω be the L-shaped domain shown in Figure 7.1; here, we set $\mathbf{j} = \mathbf{0}$ and g is chosen so that the analytical solution $\mathbf{u}$ to the two-dimensional analogue of (2.1) with $\mu \equiv \varepsilon \equiv 1$ is given, in terms of the polar coordinates (r, ϑ), by

$$\mathbf{u}(x, y) = \nabla S(r, \vartheta), \quad \text{where} \quad S(r, \vartheta) = r^{2/3} \sin(2\vartheta/3); \tag{7.2}$$

thereby, $p \equiv 0$. The analytical solution given by (7.2) contains a singularity at the corner located at the origin of Ω; here, we only have $\mathbf{u} \in H^{2/3-\varepsilon}(\Omega)^2$, $\varepsilon > 0$.

In this example, let us first confine ourselves to uniform square meshes; we shall return to the more general meshes considered in the previous example later. To this end, in Tables 7.1 and 7.2 we present a comparison of the DG–norms of the error in the approximation to both $\mathbf{u}$ and p, respectively, with the mesh function h on a sequence of uniform square meshes for $1 \leq \ell \leq 3$. In each case we show the number of elements in the computational mesh, the corresponding DG–norm of the error and the computed rate of convergence k. Here, we observe that (asymptotically) both

	$\ell = 1$		$\ell = 2$		$\ell = 3$	
Elements	$\|\boldsymbol{u} - \boldsymbol{u}_h\|_{0,\Omega}$	k	$\|\boldsymbol{u} - \boldsymbol{u}_h\|_{0,\Omega}$	k	$\|\boldsymbol{u} - \boldsymbol{u}_h\|_{0,\Omega}$	k
12	2.788e-1	-	2.420e-1	-	2.004e-1	-
48	1.817e-1	0.62	1.252e-1	0.95	9.703e-2	1.05
192	1.057e-1	0.78	6.160e-2	1.02	4.513e-2	1.10
768	6.078e-2	0.80	3.151e-2	0.97	2.187e-2	1.05
3072	3.620e-2	0.75	1.740e-2	0.86	1.154e-2	0.92

TABLE 7.3

Example 2. Convergence of $\|\boldsymbol{u} - \boldsymbol{u}_h\|_{0,\Omega}$ *on uniform square meshes with h–refinement.*

	$\ell = 1$		$\ell = 2$		$\ell = 3$	
Elements	$\|h\,\nabla_h \cdot \boldsymbol{e}_h\|_{0,\Omega}$	k	$\|h\,\nabla_h \cdot \boldsymbol{e}_h\|_{0,\Omega}$	k	$\|h\,\nabla_h \cdot \boldsymbol{e}_h\|_{0,\Omega}$	k
12	1.348e-1	-	2.086e-1	-	3.022e-1	-
48	6.438e-2	1.07	1.752e-1	0.25	2.380e-1	0.34
192	3.668e-2	0.81	1.296e-1	0.43	1.678e-1	0.50
768	2.274e-2	0.69	8.844e-2	0.55	1.115e-1	0.59
3072	1.324e-2	0.78	5.800e-2	0.61	7.206e-2	0.63

TABLE 7.4

Example 2. Convergence of $\|h\,\nabla_h \cdot \boldsymbol{e}_h\|_{0,\Omega}$ *on uniform square meshes with h–refinement.*

$\|\boldsymbol{u} - \boldsymbol{u}_h\|_{\boldsymbol{V}(h)}$ and $\|p - p_h\|_{Q(h)}$ converge to zero at the optimal rate $\mathcal{O}(h^{\min(2/3-\varepsilon,\ell)})$, as h tends to zero, predicted by Theorem 3.2.

Next, in Table 7.3 we present a comparison of the $L^2(\Omega)$–norm of the error in the numerical approximation to $\mathbf{u}$ with h. On the basis of Theorem 3.2, we expect that $\|\boldsymbol{u} - \boldsymbol{u}_h\|_{0,\Omega}$ should tend to zero at the rate $\mathcal{O}(h^{\min(2/3-\varepsilon,\ell)})$ as h tends to zero. However, from Table 7.3, we observe that for $\ell = 1, 2, 3$, the rate of convergence of the $L^2(\Omega)$–norm of the error in the approximation to $\mathbf{u}$ is slightly higher than predicted; although, asymptotically, we expect these convergence rates to slowly tend to the optimal one. Additionally, in Table 7.4 we show the convergence of $\|h\,\nabla_h \cdot \boldsymbol{e}_h\|_{0,\Omega}$ with respect to h; here, we again observe that, asymptotically, the rate of convergence tends to the one predicted in Theorem 3.4, cf. Remark 3.5. Finally, in Table 7.5 we show $\|p - p_h\|_{0,\Omega}$ for $\ell = 1, 2, 3$ based on employing uniform square meshes. In comparison with Table 7.3, Table 7.5 indicates that the rate of convergence of $\|p - p_h\|_{0,\Omega}$ is almost twice the optimal rate of $\|\boldsymbol{u} - \boldsymbol{u}_h\|_{0,\Omega}$; indeed, asymptotically, we observe that k is tending towards $4/3$ as the mesh is uniformly refined.

We remark that analogous convergence rates to those reported in Tables 7.1 – 7.5 are also observed when the numerical approximation is computed on the conforming quadrilateral meshes (i); for brevity, these results are omitted. However, convergence of the mixed DG method was *not* observed when the quadrilateral meshes (ii) were employed. We recall that the convergence proof presented in the case of weak smoothness assumptions for the component $\boldsymbol{u}$ of the analytical solution, cf. Theorem 3.2, precludes the presence of hanging nodes in the computational mesh $\mathcal{T}_h$, and, as in the case of smooth analytical solutions, assumes that the elements in $\mathcal{T}_h$ are affine. As noted above, optimal rates of convergence are still observed computationally when the quadrilateral meshes (i), which are conforming, but non-affine, are employed. In order to test the method in the case when $\mathcal{T}_h$ contains hanging nodes, but the elements are affine, we consider the performance of the mixed DG method (2.5)–(2.6) on a sequence

	$\ell = 1$		$\ell = 2$		$\ell = 3$	
Elements	$\|p - p_h\|_{0,\Omega}$	k	$\|p - p_h\|_{0,\Omega}$	k	$\|p - p_h\|_{0,\Omega}$	k
12	1.906e-1	-	1.627e-1	-	1.361e-1	-
48	1.135e-1	0.75	7.926e-2	1.04	6.327e-2	1.11
192	5.602e-2	1.02	3.452e-2	1.20	2.696e-2	1.23
768	2.487e-2	1.17	1.426e-2	1.28	1.103e-2	1.29
3072	1.049e-2	1.24	5.759e-3	1.31	4.435e-3	1.31

TABLE 7.5
Example 2. Convergence of $\|p - p_h\|_{0,\Omega}$ *on uniform square meshes with h–refinement.*

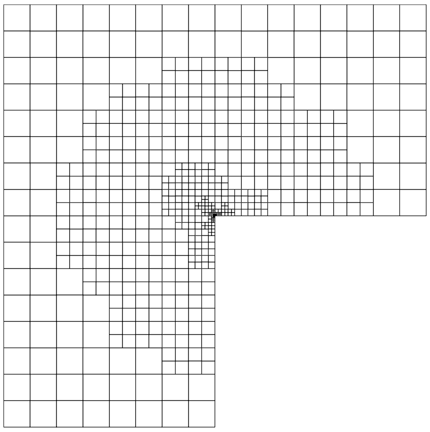

FIG. 7.9. *Example 2. Computational mesh after* 9 *adaptive refinement steps, with* 721 *nodes and* 618 *elements and* $\ell = 1$.

of adaptively refined square meshes. Here, the adaptive meshes are constructed by employing the fixed fraction strategy (with refinement and derefinement fractions set to 25% and 0%, respectively) with a simple error indicator η_K based on the gradient of the numerical approximation. More precisely, given K in $\mathcal{T}_h$, we set

$$\eta_K = \left(\|h_K \nabla \boldsymbol{u}_h\|_{0,K}^2 + \|h_K \nabla p_h\|_{0,K}^2\right)^{1/2}.$$

We remark that more sophisticated error indicators may be appropriate for this problem; here, we are simply interested in generating a sequence of adaptive meshes (containing hanging nodes), in which to test the hypotheses of our a priori error analysis. A typical mesh generated with this adaptive algorithm is shown in Figure 7.9.

In Figures 7.10 and 7.11, we present a comparison of $\|\boldsymbol{u} - \boldsymbol{u}_h\|_{\boldsymbol{V}(h)}$ and $\|p - p_h\|_{Q(h)}$, respectively, with the (square root of the) number of degrees of freedom in $\boldsymbol{V}_h \times Q_h$ for $\ell = 1$ on the sequence of adaptively refined meshes generated as above, as well as on a sequence of uniform square meshes, cf. Tables 7.1 and 7.2 above, respectively. Here, we clearly observe that the error in mixed DG discretization of (2.1) converges to zero as the finite element space $\boldsymbol{V}_h \times Q_h$ is enriched, even when the mesh contains hanging nodes; indeed, we see that the adaptively refined meshes lead to a general improvement in the error when compared to the uniform square meshes. In summary, in the case of weak Sobolev regularity assumptions on $\boldsymbol{u}$, the mixed DG method (2.5)–(2.6) is observed (numerically) to be optimally convergent on both conforming and nonconforming affine square meshes as well as on conforming non-

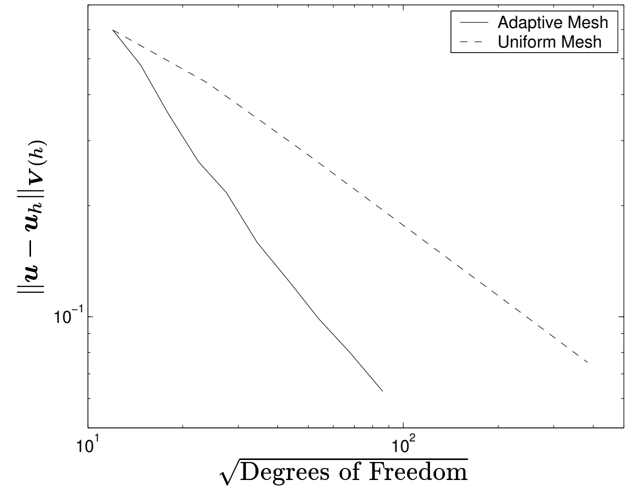

FIG. 7.10. *Example 2. Convergence of* $\|\boldsymbol{u}-\boldsymbol{u}_h\|_{\boldsymbol{V}(h)}$ *with h–refinement.*

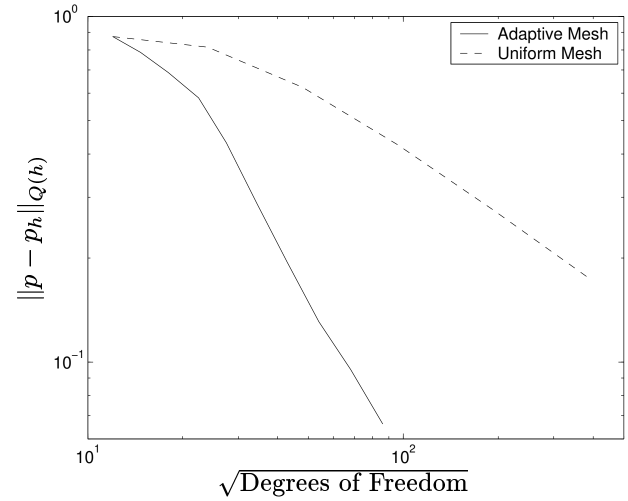

FIG. 7.11. *Example 2. Convergence of* $\|p-p_h\|_{Q(h)}$ *with h-refinement.*

affine meshes; however, convergence is not observed when the mesh contains hanging nodes *and* the elements are not affine.

8. Conclusions. In this paper, we have presented a new mixed discontinuous Galerkin method for the discretization of the time-harmonic Maxwell operator. This method is based on equal-order finite element spaces, where all the unknowns are approximated with piecewise discontinuous polynomials of the same degree. When compared to the numerical scheme proposed in [25], the amount of numerical stabilization is drastically reduced in this new method. Our error analysis and numerical results show that the method is optimally convergent in the energy norms for smooth as well as for singular solutions. In the latter case, the theoretical analysis is restricted to regular meshes without hanging nodes. However, numerical experiments for a problem with a strongly singular solution have demonstrated that the application of the method within an adaptive procedure on affine quadrilateral meshes, where hanging nodes are introduced during the course of the refinement, still leads to a convergent numerical approximation as the finite element space is enriched. A more delicate issue seems to be the one related to non-affine meshes. Indeed, our tests seem to indicate that the assumption of affineness on the meshes can not be eliminated when nonconforming meshes containing hanging nodes are employed.

Our analysis can be easily extended to the case of piecewise smooth material coefficients using the techniques in [24]. Furthermore, the application of the method to the high-frequency model in [25] is straightforward. The duality argument presented there holds for the method here and gives optimal convergence rates provided that β is large enough, but independent of the mesh size or the wave number. Future work will be devoted to the study of variants of the method that delivers optimal convergence when error in the approximation to the vector field $\boldsymbol{u}$ is measured in the $L^2(\Omega)$ norm.

Appendix A. The aim of this appendix is to prove the norm-equivalence property stated in Theorem 5.5. For the sake of simplicity, we restrict ourselves to the case of conforming meshes. For meshes with hanging nodes, under the restrictions *(i)* and *(ii)* in Section 3.2, the proof follows analogously.

A.1. Preliminaries. Writing $\widehat{K}$ to denote the reference element, let $\mathcal{N}(\widehat{K})$ be a set of nodes on the closure of $\widehat{K}$ and $\{\widehat{\varphi}_P\}_{P\in\mathcal{N}(\widehat{K})}$ the associated nodal basis of $\mathcal{S}^\ell(\widehat{K})$. Further, let $\mathcal{N}_B(\widehat{K})$ be the set of nodes in $\mathcal{N}(\widehat{K})$ that lie on $\partial\widehat{K}$. We may assume that, for each face $\widehat{f}$ of ∂K, the nodes in $\mathcal{N}_B(\widehat{K})$ belonging to the closure of $\widehat{f}$ give rise to a nodal basis of $\mathcal{S}^\ell(\widehat{f})$. For any element $K \in \mathcal{T}_h$, the corresponding sets $\mathcal{N}(K)$ and $\mathcal{N}_B(K)$, as well as the basis $\{\varphi_P^K\}_{P\in\mathcal{N}(K)}$ of $\mathcal{S}^\ell(K)$, are obtained through the affine mapping $F_K : \widehat{K} \to K$. We may also define the global sets of nodes $\mathcal{N}(\mathcal{T}_h) = \cup_{K\in\mathcal{T}_h}\mathcal{N}(K)$ and $\mathcal{N}_B(\mathcal{T}_h) = \cup_{K\in\mathcal{T}_h}\mathcal{N}_B(K)$. We assume that $\mathcal{N}(\widehat{K})$ is chosen such that, whenever K and K' are two neighboring elements with $\partial K \cap \partial K' \neq \emptyset$, the nodes of $\mathcal{N}_B(K)$ on $\partial K \cap \partial K'$ coincide with those of $\mathcal{N}_B(K')$ on $\partial K \cap \partial K'$. Thus, the set $\mathcal{N}(\mathcal{T}_h)$ allows for the construction of a global nodal basis $\{\Phi_P\}_{P\in\mathcal{N}(\mathcal{T}_h)}$ of Q_h^c (such constructions are fairly standard in the finite element theory; see, e.g., [9]). Finally, for any face $f \subset \mathcal{F}_h$, we denote by $\mathcal{N}(f)$ the set of the nodes of $\mathcal{N}_B(K)$, with K being either of the two elements sharing f, that belong to $\overline{f}$, and we may associate to $\mathcal{N}(f)$ a nodal basis of $\mathcal{S}^\ell(f)$, obtained by affinely mapping a reference face-related basis.

With this notation, we have the following two auxiliary results.

LEMMA A.1. *For $q \in Q_h$ and $K \in \mathcal{T}_h$, we have that*

$$\|\nabla q\|_{0,K}^2 \leq C\, h_K \sum_{P\in\mathcal{N}(K)} q|_K(P)^2,$$

with a constant $C > 0$ independent of the mesh size.

Proof. The bound follows from the fact that $\mathcal{N}(K)$ defines a nodal basis of $\mathcal{S}^\ell(K)$, and by employing the Cauchy-Schwarz inequality together with standard scaling arguments. □

LEMMA A.2. *If $q \in Q_h$ and $f \subset \mathcal{F}_h$ is shared by the elements K and K', we have*

$$C_1 \mathrm{h}_{|f}^2 \sum_{P\in\mathcal{N}(f)} \left[q|_K(P) - q|_{K'}(P)\right]^2 \leq \|[\![q]\!]_N\|_{0,f}^2 \leq C_2 \mathrm{h}_{|f}^2 \sum_{P\in\mathcal{N}(f)} \left[q|_K(P) - q|_{K'}(P)\right]^2,$$

with positive constants C_1 and C_2 independent of the mesh size. Here, we understand $q|_{K'}(P) = 0$ whenever $f \subset \partial K$ is a boundary face.

Proof. The equivalence follows from the fact that $\mathcal{N}(f)$ defines a nodal basis on $\mathcal{S}^\ell(f)$, the equivalence of norms in finite dimensional spaces and standard scaling arguments. □

A.2. A crucial inequality. The norm-equivalence property expressed by (5.6) is a consequence of the result proved in the following lemma. The same result can be found in [22, Lemma 3.1], but we develop here a different and constructive proof that also gives the independence of the constant with respect to the coefficients μ and ε.

LEMMA A.3. *For any $q \in Q_h$, we have*

$$\inf_{q^c \in Q_h^c} \|\varepsilon^{\frac{1}{2}} \nabla_h (q - q^c)\|_{0,\Omega} \leq C \|\mathrm{e}^{\frac{1}{2}} \mathrm{h}^{-\frac{1}{2}} [\![q]\!]_N \|_{0,\mathcal{F}_h},$$

with a constant $C > 0$ independent of the mesh size and the coefficients μ and ε.

Proof. For a node $P \in \mathcal{N}(\mathcal{T}_h)$, we set

$$\mathcal{K}(P) = \{K \in \mathcal{T}_h \,:\, P \in \mathcal{N}(K)\}, \qquad N_{\mathcal{K}}(P) = \mathrm{card}(\mathcal{K}(P)).$$

Furthermore, for $P \in \mathcal{N}_B(\mathcal{T}_h)$, we define

$$\mathcal{F}(P) = \{f \subset \mathcal{F} \,:\, P \in \mathcal{N}(f)\}, \qquad N_{\mathcal{F}}(P) = \mathrm{card}(\mathcal{F}(P)).$$

The shape-regularity assumption on the mesh guarantees that both $N_{\mathcal{K}}(P)$ and $N_{\mathcal{F}}(P)$ are bounded by a constant N, uniformly with respect to the mesh size.

Let $q \in Q_h$. Define for $P \in \mathcal{N}(\mathcal{T}_h)$

$$\overline{q}_P = \begin{cases} \dfrac{1}{N_{\mathcal{K}}(P)} \displaystyle\sum_{K' \in \mathcal{K}(P)} q|_{K'}(P) & \text{if } P \notin \Gamma, \\ 0 & \text{if } P \in \Gamma, \end{cases}$$

and let $q^c \in Q_h^c$ be the continuous interpolant given by the nodal values

$$q^c(P) = \overline{q}_P, \qquad P \in \mathcal{N}(\mathcal{T}_h).$$

By construction, we have from Lemma A.1

$$\|\nabla(q - q^c)\|_{0,K}^2 \leq C h_K \sum_{P \in \mathcal{N}_B(K)} (q|_K(P) - \overline{q}_P)^2.$$

Now, for a node $P \in \mathcal{N}_B(K)$, we obtain with the Cauchy-Schwarz inequality

$$(q|_K(P) - \overline{q}_P)^2 \leq \frac{1}{N^2} \sum_{K' \in \mathcal{K}(P)} [q|_K(P) - q|_{K'}(P)]^2.$$

Writing K_f and K'_f for the elements sharing the face f, with the convention that K'_f is void for a boundary face, we have

$$\sum_{K' \in \mathcal{K}(P)} \left[q|_K(P) - q|_{K'}(P)\right]^2 \leq C \sum_{f \in \mathcal{F}(P)} \left[q|_{K_f}(P) - q|_{K'_f}(P)\right]^2.$$

Here, we have used the shape regularity of the mesh and the uniform boundedness of $N_{\mathcal{K}}(P)$ and $N_{\mathcal{F}}(P)$; understanding that $q|_{K'_f}(P) = 0$ on boundary faces. Thus, we obtain

$$\varepsilon_K \|\nabla(q - q^c)\|_{0,K}^2 \leq C\,\varepsilon_K h_K \sum_{P\in\mathcal{N}_B(K)} \sum_{f\in\mathcal{F}(P)} \left[q|_{K_f}(P) - q|_{K'_f}(P)\right]^2.$$

Summing over all elements, taking into account the shape regularity of the mesh, yields

$$\|\varepsilon^{\frac{1}{2}}\nabla_h(q - q^c)\|_{0,\Omega}^2 \leq C \sum_{f\subset\mathcal{F}_h} \mathtt{e}_{|f}\mathtt{h}_{|f} \sum_{P\in\mathcal{N}(f)} \left[q|_{K_f}(P) - q|_{K'_f}(P)\right]^2.$$

Then, the result follows from Lemma A.2. □

A.3. Proof of Theorem 5.5. The proof of Theorem 5.5 is now straightforward. Indeed, the inequality on the right–hand side of (5.6) is trivially satisfied with $C_2 = 1$. The inequality on the left–hand side of (5.6) follows from Lemma A.3 with $C_1 = 1/\sqrt{C^2+1}$.

Acknowledgments. Paul Houston acknowledges the financial support of the EPSRC (Grant Nos: GR/K76221 and GR/R76615). This work was performed using the University of Leicester Mathematical Modelling Centre's supercomputer which was purchased through the EPSRC Strategic Equipment Initiative.

REFERENCES

[1] A. Alonso and A. Valli. A domain decomposition approach for heterogeneous time-harmonic Maxwell equations. *Comput. Methods Appl. Mech. Engrg.*, 143:97–112, 1997.

[2] A. Alonso and A. Valli. An optimal domain decomposition preconditioner for low-frequency time-harmonic Maxwell equations. *Math. Comp.*, 68:607–631, 1999.

[3] C. Amrouche, C. Bernardi, M. Dauge, and V. Girault. Vector potentials in three-dimensional non-smooth domains. *Math. Models Appl. Sci.*, 21:823–864, 1998.

[4] D.N. Arnold, F. Brezzi, B. Cockburn, and L.D. Marini. Unified analysis of discontinuous Galerkin methods for elliptic problems. *SIAM J. Numer. Anal.*, 39:1749–1779, 2001.

[5] A.S. Bonnet-BenDhia, C. Hazard, and S. Lohrengel. A singular field method for the solution of Maxwell's equations in polyhedral domains. *SIAM J. Appl. Math.*, 59:2028–2044, 1999.

[6] F. Brezzi and M. Fortin. Mixed and hybrid finite element methods. In *Springer Series in Computational Mathematics*, volume 15. Springer–Verlag, New York, 1991.

[7] F. Brezzi and M. Fortin. A minimal stabilisation procedure for mixed finite element methods. *Numer. Math.*, 89:457–491, 2001.

[8] Z. Chen, Q. Du, and J. Zou. Finite element methods with matching and nonmatching meshes for Maxwell equations with discontinuous coefficients. *SIAM J. Numer. Anal.*, 37:1542–1570, 2000.

[9] P.G. Ciarlet. *The finite element method for elliptic problems.* North–Holland, Amsterdam, 1978.

[10] B. Cockburn. Discontinuous Galerkin methods for convection-dominated problems. In T. Barth and H. Deconink, editors, *High-Order Methods for Computational Physics*, volume 9 of *Lect. Notes Comput. Sci. Engrg.*, pages 69–224. Springer–Verlag, 1999.

[11] B. Cockburn, G. Kanschat, D. Schötzau, and C. Schwab. Local discontinuous Galerkin methods for the Stokes system. *SIAM J. Numer. Anal.*, 40:319–343, 2002.

[12] B. Cockburn, G.E. Karniadakis, and C.-W. Shu. The development of discontinuous Galerkin methods. In B. Cockburn, G.E. Karniadakis, and C.-W. Shu, editors, *Discontinuous Galerkin Methods: Theory, Computation and Applications*, volume 11 of *Lect. Notes Comput. Sci. Engrg.*, pages 3–50. Springer–Verlag, 2000.

[13] B. Cockburn, G.E. Karniadakis, and C.-W. Shu, editors. *Discontinuous Galerkin Methods. Theory, Computation and Applications*, volume 11 of *Lect. Notes Comput. Sci. Engrg.* Springer–Verlag, 2000.

[14] B. Cockburn and C.-W. Shu. Runge–Kutta discontinuous Galerkin methods for convection–dominated problems. *J. Sci. Comp.*, 16:173–261, 2001.

[15] M. Costabel and M. Dauge. Weighted regularization of Maxwell equations in polyhedral domains. Technical Report 01-26, IRMAR, University of Rennes, 2001. Numer. Math. (to appear).

[16] L. Demkowicz and L. Vardapetyan. Modeling of electromagnetic absorption/scattering problems using *hp*–adaptive finite elements. *Comput. Methods Appl. Mech. Engrg.*, 152:103–124, 1998.

[17] P. Fernandes and G. Gilardi. Magnetostatic and electrostatic problems in inhomogeneous anisotropic media with irregular boundary and mixed boundary conditions. *Math. Models Methods Appl. Sci.*, 7:957–991, 1997.

[18] P. Hansbo and M. Larson. Discontinuous finite element methods for incompressible and nearly incompressible elasticity by use of Nitsche's method. *Comput. Methods Appl. Mech. Engrg.*, 191:1895–1908, 2002.

[19] P. Houston, I. Perugia, and D. Schötzau. *hp*-DGFEM for Maxwell's equations. Technical Report 02-02, University of Basel, Department of Mathematics, 2002.

[20] P. Houston, C. Schwab, and E. Süli. Discontinuous *hp*-finite element methods for advection–diffusion–reaction problems. *SIAM J. Numer. Anal.*, 40:2133–2163, 2002.

[21] D.A. Kopriva, S.L. Woodruff, and M.Y. Hussaini. Discontinuous spectral element approximation of Maxwell's equations. In B. Cockburn, G.E. Karniadakis, and C.-W. Shu, editors, *Discontinuous Galerkin Methods. Theory, Computation and Applications*, volume 11 of *Lect. Notes Comput. Sci. Eng.*, pages 355–361. Springer–Verlag, 2000.

[22] M. Larson and A. Niklasson. Conservation properties for the continuous and discontinuous Galerkin method. Technical Report 2000-08, Chalmers Finite Element Center, Chalmers University, 2000.

[23] J.C. Nédélec. A new family of mixed finite elements in $\mathbb{R}^3$. *Numer. Math.*, 50:57–81, 1986.

[24] I. Perugia and D. Schötzau. The *hp*-local discontinuous Galerkin method for low-frequency time-harmonic Maxwell's equations. Technical Report 1774, IMA, University of Minnesota, 2001. Math. Comp. (to appear).

[25] I. Perugia, D. Schötzau, and P. Monk. Stabilized interior penalty methods for the time-harmonic Maxwell equations. Technical Report 101, MSI, University of Minnesota, 2001. Comput. Methods Appl. Mech. Engrg. (to appear).

[26] B. Rivière, M. F. Wheeler, and V. Girault. A priori error estimates for finite element methods based on discontinuous approximation spaces for elliptic problems. *SIAM J. Numer. Anal.*, 39:901–931, 2001.

[27] B. Rivière, M.F. Wheeler, and V. Girault. Improved energy estimates for interior penalty, constrained and discontinuous Galerkin methods for elliptic problems, Part I. *Computational Geosciences*, 3:337–360, 1999.

[28] D. Schötzau, C. Schwab, and A. Toselli. Mixed *hp*-DGFEM for incompressible flows. Technical Report 02-10, Seminar for Applied Mathematics, ETH Zürich, 2002. SIAM J. Numer. Anal. (to appear).

[29] A. Toselli. *hp*-discontinuous Galerkin approximations for the Stokes problem. *Math. Models Methods Appl. Sci.*, 12:1565–1616, 2002.

[30] L. Vardapetyan and L. Demkowicz. *hp*-adaptive finite elements in electromagnetics. *Comput. Methods Appl. Mech. Engrg.*, 169:331–344, 1999.

[31] T. Warburton and J.S. Hesthaven. High-order/spectral methods on unstructured grids, I. Time-domain solution of Maxwell's equations. J. Comput. Phys. (to appear).